UNIVERSIDAD NACIONAL AUTÓNOMA DE MÉXICO

FACULTAD DE INGENIERÍA

APPLICATION OF AN IMPROVED SEQUENTIALLY LINEAR ANALYSIS MODEL TO THE APPROXIMATION OF THE NON-LINEAR BEHAVIOUR OF STRUCTURES

TESIS

Que para obtener el título de

INGENIERIA CIVIL

P R E S E N T A

Oliva Núñez Vargas

DIRECTOR DE TESIS

Dr. Héctor Rodrigo Amezcua Rivera

Ciudad Universitaria, Cd. Mx., 2023

Acknowledgments

I would like to express my special thanks and gratitude to my sister, Itzel, who it is not only part of my family, but also a friend, partner that I would always count on.

I would also like to extend my gratitude to Rodrigo, who has been an incredible teacher with great talent, patience, and the will of making me his student. Because he has been a leader that shows the way for his disciples.

My sincere thank also to Dr. Ayala, who has taught me that engineering is also music for the soul, and that if I have seen more, it is because I am sitting on the shoulders of giants.

To my parents, for the foundations of my education.

To the Faculty of Engineering and the University, for giving me everything that I have never believed I could have.

Abstract

Nowadays, the new design philosophies of structures contemplate the possibility that some of the elements that compose them present damage due to various requests to which they are subjected, for example, seismic events. In order to consider the damage in the structures, it is necessary that the structural analysis consider the non-linear behavior of the materials, at least in a simplified way.

The Finite Element Method (FEM) is a numerical procedure commonly used in the study of problems in various areas of engineering. The FEM is used to obtain numerical approximations of problems that are too complex to be solved analytically, for example, the nonlinear analysis of structures. In this work, the FEM is used together with a strategy based on Linear Sequential Analysis (ALS) in the study of the nonlinear behavior of material structures with quasi-brittle behavior in a computationally efficient way.

Throughout the document several application examples with different configurations and parameters are studied. The results obtained are compared with other methods and with experimental evidence. Additionally, a modification to the softening law of the material is proposed that allows obtaining results closer to what was observed in the experiments.

Resumen

En la actualidad, las nuevas filosofías de diseño de estructuras contemplan la posibilidad de que algunos de los elementos que las componen presenten daño ante diversas solicitaciones a las que son sometidas, por ejemplo, eventos sísmicos. Para considerar el daño en las estructuras, es necesario que el análisis estructural considere el comportamiento no-lineal de los materiales cuando menos de manera simplificada.

El Método de los Elementos Finitos (MEF) es un procedimiento numérico comúnmente empleado en el estudio de problemas en diversas áreas de la ingeniería. El MEF se utiliza para obtener aproximaciones numéricas de problemas que son demasiado complejos para resolverlos analíticamente, por ejemplo, el análisis no-lineal de estructuras. En este trabajo, se emplea el MEF en conjunto con una estrategia basada en Análisis Lineales Secuenciales (ALS) en el estudio del comportamiento no-lineal de estructuras de materiales con comportamiento cuasi-frágil de manera computacionalmente eficiente.

A lo largo del documento se estudian diversos ejemplos de aplicación con configuraciones y parámetros distintos. Los resultados obtenidos se comparan con otros métodos y con evidencia experimental. Adicionalmente, se propone una modificación a la ley de ablandamiento del material que permite la obtención de resultados más cercanos a lo observado en experimentos.

List of figures

List of Tables

Contents

Introduction

Problem statement

The problem of analyzing the non-linear behaviour of materials, such as concrete, masonry or steel, can be studied by the plasticity theory which considers the appearance of permanent deformations. Additionally, this theory can contemplate that certain materials become stronger once they start to yield, *i.e.* hardening, or, in the other hand, that they become weaker, *i.e.* softening. For the second premise, the procedure called Sequentially Linear Analysis (SLA) can be also applied to get a computationally efficient damage prediction.

The non-linear analysis of structures through the Finite Element Method (FEM) starts by the discretization of the structure subjected to external forces into elements of simpler geometry composed of deformable materials. Each of these elements contribute to the general behaviour of the structure by being submitted to forces that change the original configuration of such structure. During this process, linear-elastic or plastic deformations can appear. To obtain numerical results closer to the ones obtained by laboratory tests, in this thesis the SLA procedure are employed.

Objectives

The main objective of this work is to improve, apply and validate a finite element model for the approximation of the nonlinear behaviour of structures, based on sequentially linear analysis and implemented through a stabilized reduced integration scheme for 4-node quadrilateral elements, through the proposal of a new softening law.

In order to achieve the main objective, the following specific tasks were stablished:

- Study the general basis of the Finite Element Method (FEM) emphasizing in the isoparametric formulation of the 4-node quadrilateral finite element.

- Perform linear analysis and convergence analysis employing the Scientific ToolKit for OpenSees software (STKO) to assimilate how the method works.
- Study and discuss the effect of the use of different numerical integration schemes in the computation of the stiffness matrix of a 4-node quadrilateral element and
- Study and Stabilized Reduced Integration (SRI) scheme for the 4-node quadrilateral finite element which allows the use of low-order integration rules with numerical stability.
- Study the procedure based on SLA aimed to approximate the non-linear behaviour of quasi-fragile materials.
- Apply and validate the strategy composed by both SLA and SRI through its application to several examples.
- Validate the procedure through the study of a plate previously tested in laboratory, analyzing different scenarios, assigning various characteristics associated with the geometry, methodology of the case or even the parameters implemented in the analysis.
- Propose a new softening law which improve the behaviour approximated in the previous specific task.

Outline of the thesis

The contents of this thesis are divided in three different parts. The first one discusses the FEM basis from the generation process of the mesh to the use of different Gauss-Legendre quadrature rules to obtain the stiffness. The second part describes the SLA which uses a softening law making an iterative process where the element that belongs to the model crack path have degraded properties. The last section is the main section of this thesis, where a specific example is included.

Regarding the SLA procedure, for a saw-tooth softening law, it must require that the area enclosed by the saw tooth equals the area enclosed by the base material laws. This SLA procedure includes an iterative procedure that makes FEM determine the stiffness, loads and displacements results, but this is only a part of the method. A second requirement includes solving through SLA procedure by making a damage band where every element belonging to the area can be selected as the weakest element, as a result the load and deformation are computed, and the model is ready to make another analysis.

The application example is a tension plate tested by Van Vliet (2000), where he expected to have a geometry of a concrete plate which have the highest stress concentration in the center of such plate. For this purpose, Van Vliet (2000) analyzed 6 different specimens with different depth and

all the dimensions of the geometry, for this test, a C specimen was chosen to compare the most desirable approach by considering non-equivalent characteristics.

Chapter I
Finite Element Method

I.I Introduction

The Finite Element Method (FEM) is a numerical tool used to, among other applications, approximate the behaviour of structures through the discretization of the complicated geometry of such structure in elements of simpler geometry, *e.g.*, triangles or quadrilaterals for two-dimensional analysis or hexahedrals for three-dimensional analysis among others (Bathe, 2006).

There are several possible mesh configurations to analyse the behaviour of the structure. For example, Figure 1.1 describes how Orduña *et. al.* (2007) discretized the arcade of the monastery of São Vicente de Fora to estimate the seismic vulnerability of the monastery (Amezcua, 2016).

a) b)

Figure 1.1 Geometry of the monastery of Saó Vicente de Fora: a) photography and b) finite-element mesh (Orduña et al., 2007)

If the mesh is fine, which means that contains a high quantity of elements on it, the problem is harder to resolve (fig. 2.1b). In the other hand, a more simplified mesh, *i.e.*, a coarse mesh with a reduced number of elements, helps to have an easier way to analyse the problem. In terms of results, it is expected that a finer mesh has a better approximation of the solution.

In other words, the configuration of different meshes, *e.g.*, size, type, disposition, and quantity of elements, of the structure defines the quality of the approximation of the solution of the mathematically modeled problem. As expected, for a significantly fine mesh the results are closer to reality but, also, computationally demanding (Gupta & Meek, 1996).

The 4-node quadrilateral element is used in all the examples included in this thesis. For this reason, this chapter begins with a brief description of the formulation of a quadrilateral element. Subsequently, the stiffness matrix, through different integration schemes is obtained to discuss the differences between them. Also, an example of a problem is solved by a widely used software.

I.II Isoparametric formulation of the 4-node quadrilateral element

In the context of the FEM, the shape functions describe the behaviour of every node of certain element. The quantity of the shape functions (x, y) is equal to the number of nodes of the quadrilateral. Considering only a middle node of an element means that only one shape function is required (fig. 2.2a). If one node for each apex is considered, four shape functions need to be contemplated in the problem (fig. 2.1b). Additionally, for a quadrilateral with middle nodes between the edges and another ubicated in the center of the quadrilateral, the number of shape functions increase to nine (fig. 2.2).

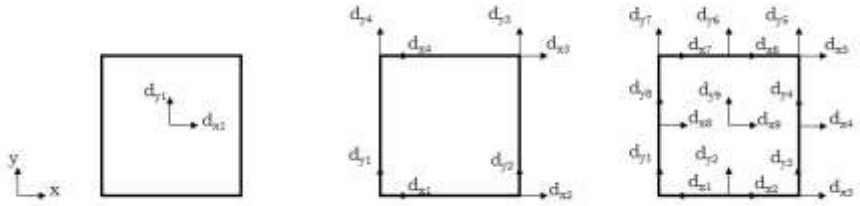

a) b) c)

Figure 1.1. Examples of nodes considered in a quadrilateral finite element: a) 1-node, b) 4-node and c) 9-node

To change the variables to other different coordinate system in which the problem can have an equivalent but simpler form, natural coordinates are used. For this purpose, shape functions are transformed in terms of (ξ, η). For example, the geometrical representation of this transformation can be observed for a 9-node quadrilateral finite element in fig. 2.3.

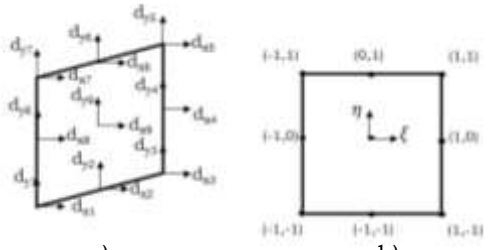

a) b)

Figure 1.3. Quadrilateral Coordinates transformation of a 9-node quadrilateral element: a) global and b) natural system

The shape functions are employed on the compatibility matrix construction, **B**, which is given by the eq. 2.1. The geometry of the analyzed element and the number of nodes define the size of the matrix according to the degrees of freedom. As mentioned above, this research is focused on the employment of 4-node quadrilateral elements. Therefore, in this formulation two displacements and forces at each node are considered (Juárez, 2012), (eq. 2.1).

$$\mathbf{B} = \frac{1}{|\mathbf{J}|}\begin{Bmatrix} y_i^T\tau & 0 \\ 0 & -x_i^T\tau \\ -x_i^T\tau & y_i^T\tau \end{Bmatrix} \tag{2.1}$$

Where y_i and x_i, are the shape functions of every node in global coordinates. τ is an antimetric matrix and $|\mathbf{J}|$ is the Jacobian to make the change of global to natural coordinates.

To describe a numerical example, the 4-node quadrilateral of fig. 2.4 is considered. The load is applied at the top nodes of the element and the restrains are at the bottom.

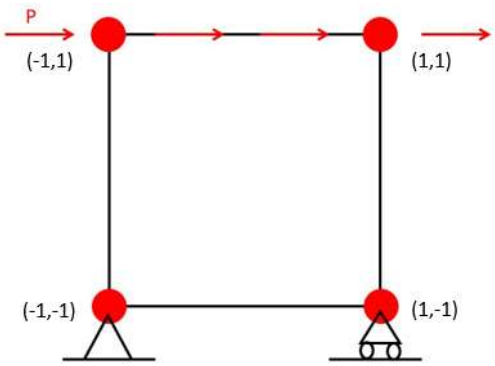

Figure 1.4. 4-node quadrilateral element considered

The **B** matrix of a 4-node quadrilateral element can be represented as (eq. 2.2):

$$\mathbf{B}(\xi,\eta) = \begin{bmatrix} 0.5\eta-0.5 & 0 & 0.5-0.5\eta & 0 & 0.5\eta+0.5 & 0 & -0.5\eta-0.5 & 0 \\ 0 & 0.5\xi-0.5 & 0 & -0.5\xi-0.5 & 0 & 0.5\xi+0.5 & 0 & 0.5-0.5\xi \\ 0.5\xi-0.5 & 0.5\eta-0.5 & -0.5\xi-0.5 & 0.5-0.5\eta & 0.5\xi+0.5 & 0.5\eta+0.5 & 0.5-0.5\xi & -0.5\eta-0.5 \end{bmatrix} \tag{2.2}$$

Furthermore, the constitutive matrix, **C**, is given by the λ and μ parameters of Lamé (eq. 2.3).

For the material properties of the elements, such as the Young's Modulus (E) and the Poisson's Ratio (ν), a constitutive matrix for plane stress is defined as (eq. 2.4):

$$\boldsymbol{C} = \begin{Bmatrix} \lambda+2\mu & \lambda & \lambda & 0 & 0 & 0 \\ \lambda & \lambda+2\mu & \lambda & 0 & 0 & 0 \\ \lambda & \lambda & \lambda+2\mu & 0 & 0 & 0 \\ 0 & 0 & 0 & \mu & 0 & 0 \\ 0 & 0 & 0 & 0 & \mu & 0 \\ 0 & 0 & 0 & 0 & 0 & \mu \end{Bmatrix} \tag{2.3}$$

$$\boldsymbol{C} = \frac{E}{1-\nu^2}\begin{bmatrix} 1 & \nu & 0 \\ \nu & 1 & 0 \\ 0 & 0 & \frac{1-\nu}{2} \end{bmatrix} \tag{2.4}$$

For example, for a Young's Modulus $E = 1000$ kg/cm^{2}and a Poisson's Ratio $\nu = 0.2$ the constitutive matrix for plane stress becomes (eq. 2.5):

$$\boldsymbol{C} = \begin{bmatrix} 1.04 \times 10^3 & 208.33 & 0 \\ 208.33 & 1.04 \times 10^3 & 0 \\ 0 & 0 & 416.67 \end{bmatrix} \frac{kg}{cm^2} \tag{2.5}$$

According to kinematics, stiffness is the property of the element to resist displacements when applying a force. In the FEM, the stiffness matrix, $\boldsymbol{K}$, is represented by an integral of a function computed by the product of the transposed compatibility matrix, the constitutive matrix, and the compatibility matrix (eq. 2.6):

$$\boldsymbol{K} = \int_{\Omega} \boldsymbol{B}^T \boldsymbol{C}\boldsymbol{B}\, d\Omega = t \int_{A} \boldsymbol{B}^T \boldsymbol{C}\boldsymbol{B}\, dA = t \int_{-1}^{1} \int_{-1}^{1} \boldsymbol{B}(\xi,\eta)^T \boldsymbol{C}\boldsymbol{B}(\xi,\eta)\, |\boldsymbol{J}|\, d\xi d\eta \tag{2.6}$$

Where t is the thickness, or the smallest dimension of the specimen to be analyzed. To obtain the result of the integral of eq. 2.6 on an interval [-1,1] a Gauss-Legendre quadrature is used, *i.e.*, numerical integration, which is an integration method to show a mathematical approximation of the real problem where the expression is computed as (eq. 2.7):

$$\mathbf{K} = \int_{\Omega} \mathbf{B}^T \mathbf{C}\mathbf{B}\, d\Omega = t \sum_{i=1}^{n} \sum_{j=1}^{n} \phi(\xi_i, \eta_j)\omega_i\omega_j\, |\mathbf{J}| \tag{2.7}$$

Where n is the number of integration points, ξ_i and η_j are the sampling points, and ω_i and ω_j are the assigned weights per sampling point which values are expressed in the following table:

Table 2.1. Gauss-Legendre quadrature for one and two integration points

n	ξ_i, η_j	w_i, w_j
1	0	2
2	$\pm\frac{1}{\sqrt{3}}$	1

Evaluating the integral of eq.2.7 by means of numerical integration employing 4 integration points through Gauss-Legendre quadrature, a stiffness matrix is obtained whose dimension is given by the number of degrees of freedom per node (eq. 2.8). The stiffness matrix of eq. 2.8 is defined as a singular matrix. The subtract from the number of the rows or the columns minus the range of the matrix is equal to the number of restraints that need to be imposed.

$$\mathbf{K} = \begin{bmatrix} 486.11 & 156.25 & -277.78 & 156.25 & -277.78 & -156.25 & 34.72 & 52.08 \\ 156.25 & 486.11 & 52.08 & 34.72 & -156.25 & -243.06 & -52.08 & -277.78 \\ -277.78 & 52.08 & 486.11 & -156.25 & 34.72 & -52.08 & -243.06 & 156.25 \\ -52.08 & 34.72 & -156.25 & 486.11 & 52.08 & -277.78 & 156.25 & -243.06 \\ -243.06 & -156.25 & 34.72 & 52.08 & 486.11 & 156.25 & -277.78 & -52.08 \\ -156.25 & -243.06 & -52.08 & -277.78 & 156.25 & 486.11 & 52.08 & 34.72 \\ 34.72 & -52.08 & -243.06 & 156.25 & -277.78 & 52.08 & 486.11 & -156.25 \\ 52.08 & 277.78 & 156.25 & -243.06 & -52.08 & 34.72 & -156.25 & 486.11 \end{bmatrix} \quad (2.8)$$

Consequentially, to obtain the displacements of the quadrilateral element of fig 2.4 it is necessary to obtain a non-singular stiffness matrix by the imposition of the boundary conditions. Once the nodes with fixed restraints are determined in the quadrilateral element and a non-singular stiffness matrix is obtained, the next step is to compute the inverse matrix. For example, for a bottom-restrained quadrilateral, the inverse matrix is (eq. 2.9):

$$\mathbf{K}^{-1} = \begin{bmatrix} 0.0051 & -0.0022 & 0.0038 & 0.0019 \\ -0.0022 & 0.0030 & -0.0019 & -0.0011 \\ 0.0038 & -0.0019 & 0.0051 & 0.0022 \\ 0.0019 & -0.0011 & 0.0022 & 0.0030 \end{bmatrix} \frac{cm}{kg} \quad (2.9)$$

The inverse of the stiffness matrix (eq. 2.9) multiplied by the force vector, p, gives the displacements, d (eq. 2.10):

$$d = \mathbf{K}^{-1} p \quad (2.10)$$

Where the displacements results are (eq. 2.11):

$$d = \begin{bmatrix} 0.0089 \\ -0.0041 \\ 0.0089 \\ 0.0041 \end{bmatrix} cm \tag{2.11}$$

To obtain strains, ε, the expression is given by (eq. 2.12):

$$\varepsilon = \mathbf{B}d \tag{1.12}$$

In this case, for a unit force applied at the nodes above the quadrilateral, strain results are (eq. 2.13):

$$\varepsilon_1 = \begin{bmatrix} 0 \\ -0.0024 \\ 0.0024 \end{bmatrix} \varepsilon_2 = \begin{bmatrix} 0 \\ 0.0024 \\ 0.0072 \end{bmatrix} \varepsilon_3 = \begin{bmatrix} 0 \\ 0.0024 \\ 0.0024 \end{bmatrix} \varepsilon_4 = \begin{bmatrix} 0 \\ -0.0024 \\ 0.0072 \end{bmatrix} \tag{2.13}$$

In terms of stress results, constitutive matrix per strain vector will give them (eq. 2.14):

$$\sigma = \mathbf{C}\varepsilon_i \tag{2.14}$$

And the results are (eq. 2.15):

$$\sigma_1 = \begin{bmatrix} -0.4949 \\ -2.4744 \\ 1.0103 \end{bmatrix} \varepsilon_2 = \begin{bmatrix} 0.4949 \\ 2.4744 \\ 2.9897 \end{bmatrix} \varepsilon_3 = \begin{bmatrix} \begin{Bmatrix} 0.4949 \\ 2.4744 \\ 1.0103 \end{Bmatrix} \end{bmatrix} \varepsilon_4 = \begin{Bmatrix} -0.4949 \\ -2.4744 \\ 2.9897 \end{Bmatrix} \tag{2.15}$$

I.III Full and reduced numerical integration

In the above section, four integration points are used. When the stiffness matrix of a quadrilateral is computed employing only one integration point is called reduced integration (RI) (fig 2.5).

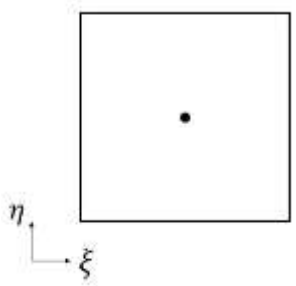

Figure 1.5. Reduced integration in the 4-node quadrilateral element

Furthermore, it is well known that a 4-node quadrilateral finite element have eight deformation modes. When full integration (FI) is used, the first three modes have a rigid-body behaviour (fig. 2.6). The following two are the known as bending modes (fig. 2.7), and the last three, have are the constant strain modes (fig. 2.8).

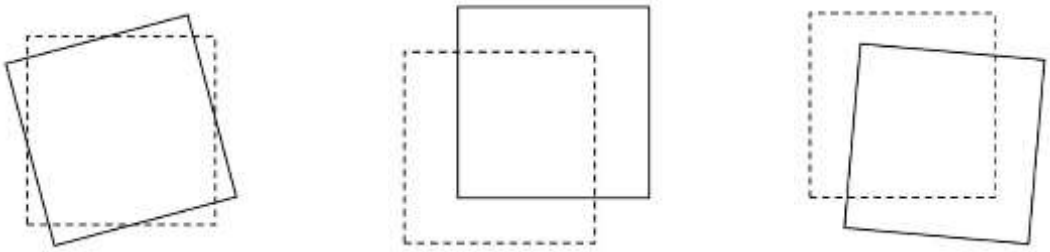

a) b) c)

Figure 1.6. Rigid-body modes

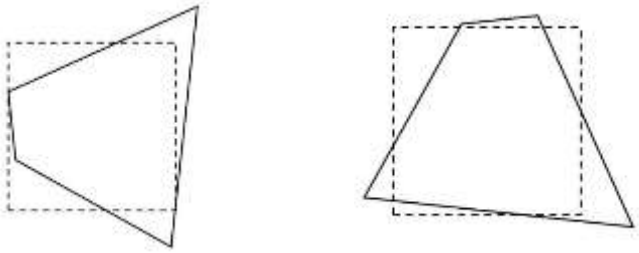

d) e)

Figure 1.7. Bending modes

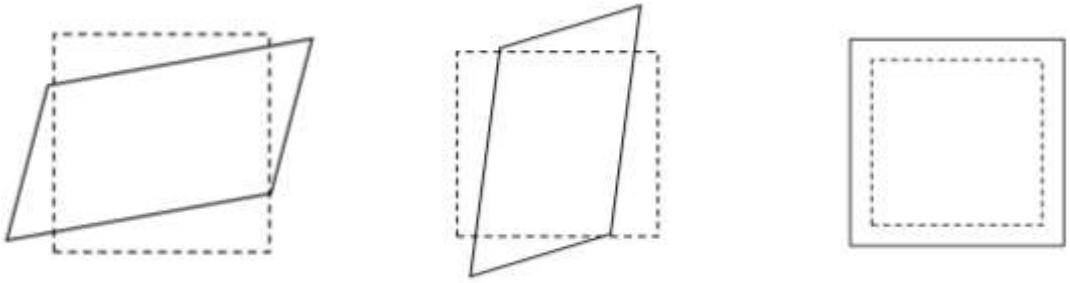

a) b) c)

Figure 1.8. Constant-strain modes

When reduced integration is employed, hourglass modes appear. The first five modes are zero-energy deformation modes, but they do not have a rigid-body behaviour (fig. 2.9). On the other hand, the last three modes are the same as when full integration is used (fig. 2.10).

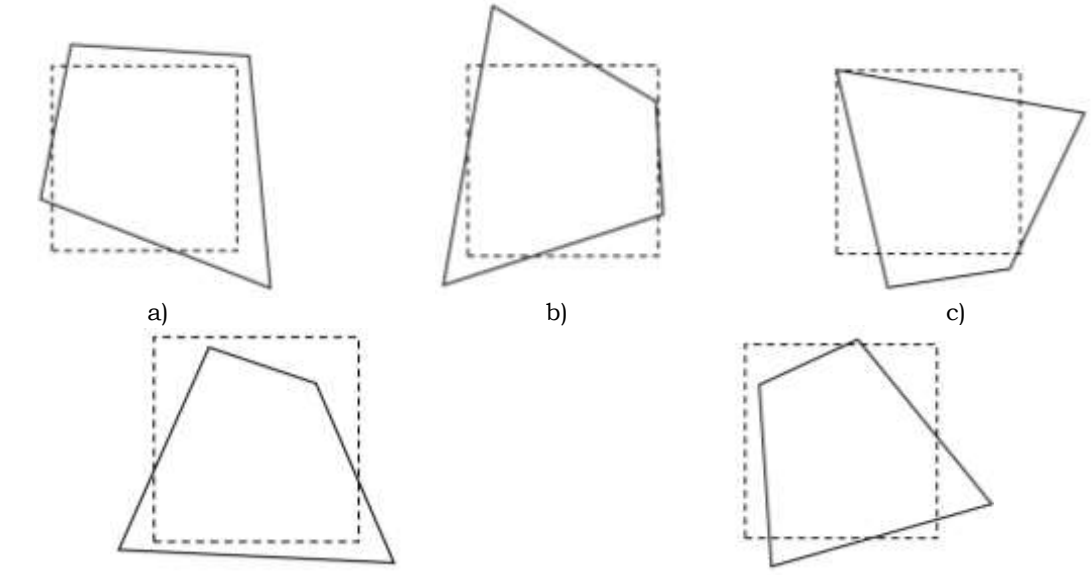

Figure 1.9. Hourglass modes

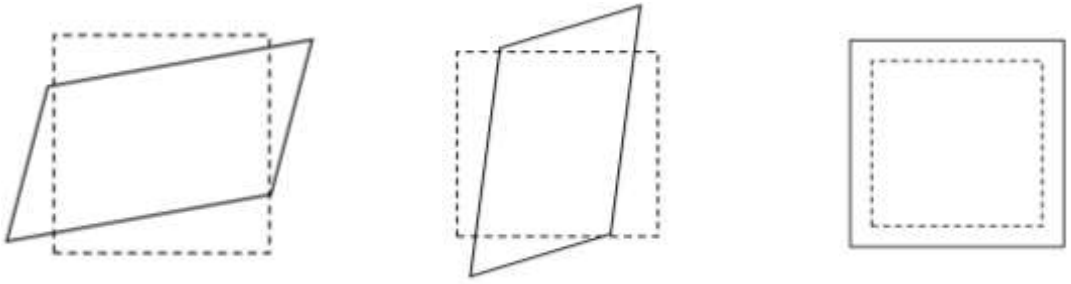

Figure 1.10. Constant-strain modes

I.IV Stabilization procedure for reduced integration

It is demonstrated that the rate of convergence of the one-point quadrature element is comparable to that of the fully integrated elements (Belytschko et al., 1978). The principal disadvantage of full integration is related to incompressibility of materials which can be fixed by employing reduced integration. On the other hand, the use of reduced integration leads to numerically unstable sub-integrated stiffness matrix. The problem to solve is that this matrix has an order less than that required, i.e., rank-deficient matrices. The hourglass control method is used to increase the rank of the

one-point stiffness matrix from 3 to 5 by adding an stabilizer matrix (Jacquotte et al., 1986).

One of the stabilization procedures developed was studied by Belytschko and Liu (1978). In terms of the mathematical method, the stabilizer matrix augments the rank of the stiffness matrix from 3 to 5 though adding neglected terms in the reduced integration procedure. Furthermore, the hourglass modes becomes rigid-body and bending modes (Amezcua, 2023) (eq. 2.16):

$$\mathbf{K} = \mathbf{K}_{(1)} + \mathbf{K}_{stab} \tag{2.16}$$

In eq. 2.16, $\mathbf{K}_{(1)}$ is the stiffness matrix that have an deficient rank that depends on the area on the element A, the thickness of the element t, the strain-displacement matrix $\mathbf{B}_{(1)}$ evaluated in one integration point and $\mathbf{C}$, the constitutive matrix. Moreover, the stabilizer matrix $\mathbf{K}_{stab}$ can be calculated as (eq. 2.17):

$$\mathbf{K}_{stab} = t \int_A \mathbf{B}_{stab}^T \mathbf{C} \mathbf{B}_{stab} \, dA \tag{2.17}$$

Where $\mathbf{B}_{stab}$ stands for the strain-displacement matrix (Amezcua, 2023) and can be obtained as (eq. 1.18):

$$\mathbf{B}_{stab} = \begin{bmatrix} h_{,x}\gamma_1 & 0 & h_{,x}\gamma_2 & 0 & h_{,x}\gamma_3 & 0 & h_{,x}\gamma_4 & 0 \\ 0 & h_{,y}\gamma_1 & 0 & h_{,y}\gamma_2 & 0 & h_{,y}\gamma_3 & 0 & h_{,y}\gamma_4 \\ h_{,x}\gamma_1 & h_{,x}\gamma_1 & h_{,x}\gamma_2 & h_{,x}\gamma_2 & h_{,x}\gamma_3 & h_{,x}\gamma_3 & h_{,x}\gamma_4 & h_{,x}\gamma_1 \end{bmatrix} \tag{2.18}$$

In the previous equation, h is the product of the natural coordinates, $h = \xi\eta$ and the comma stands for the lower-case subscripts in terms of partial differentiation with respect to the global coordinate system (x, y) (Amezcua, 2022). Flanagan and Belytschko (1981) defined the gamma terms as the components of the hourglass shape vector.

Also, the $\mathbf{K}_{stab}$ can be obtained as (eq. 2.19):

$$\mathbf{K}_{stab} = t \begin{bmatrix} (C_{11}H_{xx} + C_{33}H_{yy})\gamma\gamma^T & ((C_{12} + C_{33})H_{xy})\gamma\gamma^T \\ ((C_{12} + C_{33})H_{xy})\gamma\gamma^T & (C_{11}H_{yy} + C_{33}H_{xx})\gamma\gamma^T \end{bmatrix} \tag{2.19}$$

Where C_{ij} are the elements of the plane stress or plane strain of the constitutive matrix and H_{xx}, H_{yy} and H_{xy} are obtained by the eq. 2.10 (Belytschko and Bachrach, 1986). Moreover, when K_{stab} is computed through numerical integration, it is necessary to use a 2 x 2 Gauss-

Legendre quadrature to numerically evaluate H_{xx}, H_{yy} and H_{xy}. Thus, for a one integration point, the domain of the H_{xx}, H_{yy} and H_{xy} equations change to that of the natural coordinate system and can be obtained as (eqs. 2.20a to 2.20c) (Amezcua, 2023):

$$H_{xx} = \int_{-1}^{+1}\int_{-1}^{+1} h_{,x}^2 |\mathbf{J}| d\xi\, d\eta \tag{2.20a}$$

$$H_{yy} = \int_{-1}^{+1}\int_{-1}^{+1} h_{,y}^2 |\mathbf{J}| d\xi\, d\eta \tag{2.20b}$$

$$H_{xy} = \int_{-1}^{+1}\int_{-1}^{+1} h_{,x} h_{,y} |\mathbf{J}| d\xi\, d\eta \tag{2.20c}$$

Additionally, Amezcua (2023) describes that $h_{,x}$ and $h_{,y}$ can be computed as (eqs. 2.21a and 2.21b).

$$h_{,x} = -\frac{4}{\beta}(y\,\alpha_1\xi - y\,\alpha_3\eta) \tag{2.21a}$$

$$h_{,y} = -\frac{4}{\beta}(x\,\alpha_1\xi - x\,\alpha_3\eta) \tag{2.21b}$$

Where β is an equation that depends on three different constants (eq. 2.22):

$$\beta = \delta_1 + \delta_2\xi + \delta_3\eta \tag{2.22}$$

And the δ_n can be computed as the eqs. 2.23a to 2.23c show:

$$\delta_1 = (x\alpha_1)(y\alpha_3) - (x\alpha_3)(y\alpha_1) \tag{2.23a}$$
$$\delta_2 = (x\alpha_1)(y\alpha_2) - (x\alpha_2)(y\alpha_1) \tag{2.23b}$$
$$\delta_3 = (x\alpha_2)(y\alpha_3) - (x\alpha_3)(y\alpha_2) \tag{2.23c}$$

Where eq. 2.24a to 2.24c demonstrates how to obtain the alpha vector:

$$\alpha_1^T = [-1 \quad 1 \quad 1 \quad -1] \tag{2.24a}$$
$$\alpha_2^T = [1 \quad -1 \quad 1 \quad -1] \tag{2.24b}$$
$$\alpha_3^T = [-1 \quad -1 \quad 1 \quad 1] \tag{2.24c}$$

I.V Linear FEM analysis

The theorical and mathematical basis of the FEM were reviewed in the previous section. It is clear that in order to apply the FEM to the structural

analysis, a numerical implementation is required. There are several computational tools that can help engineers to apply the FEM to the mentioned task. One of the most popular is OpenSees. This open source is a software framework for developing applications to simulate the performance of structural and geotechnical systems.

Additionally, there are complementary developments for OpenSees, such as the Scientific ToolKit for OpenSees (STKO) which is an advanced Graphical User Interface (GUI) for OpenSees.

In the following lines, a brief description of the STKO software (ASDEA Software, 2018), is included. For a 4-node finite quadrilateral the main algorithm needs to define the geometry that can be created with a *Face* $\frac{3}{4}$ *option*. This option is the one that helps to draw the geometry in the software (fig.2.11).

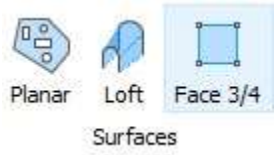

Figure 1.11. Screenshot of Face ¾ option in STKO software (ASDEA software, 2018)

Also, to define the type of analysis, it is used *Linear Time Series option* (fig.2.12).

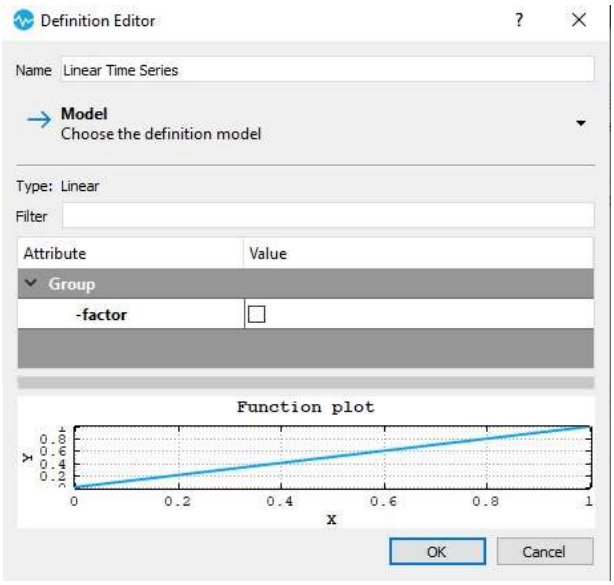

Figure 1.12. Screenshot of Linear Time Series in STKO software (ASDEA software, 2018)

Moreover, the mechanical properties of the material that need to be assigned are defined as an *Elastic Isotropic*. The material properties that were used in this example are the following: a Young Modulus of $E = 221359.436 kg/cm^3$, as the concrete, and a Poisson Ratio of $\nu = 0.2$ (fig 2.13), to exemplify a real example.

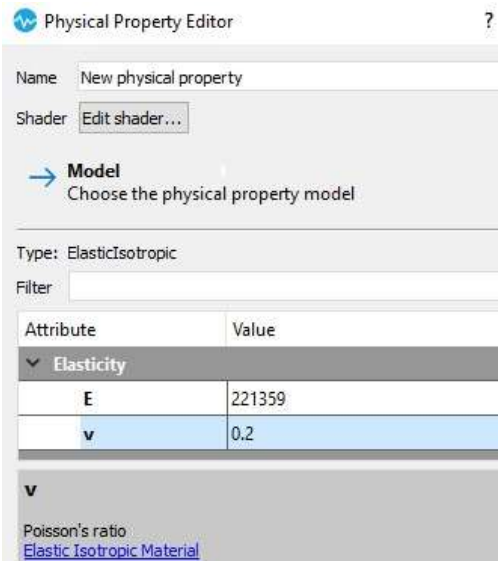

Figure 1.13. Screenshot of Material Properties in STKO software (ASDEA software, 2018)

Then, the element property defined as an *enhanced quad* (option in the software used to define the kind of strain in the figure would be submitted with a unit thickness) is selected (fig 2.14).

Figure 1.14. Screenshot of Element property in STKO software (ASDEA software, 2018)

In addition, a horizontal force acting at the above nodes and two restraints at the bottom are applied (fig. 2.15).

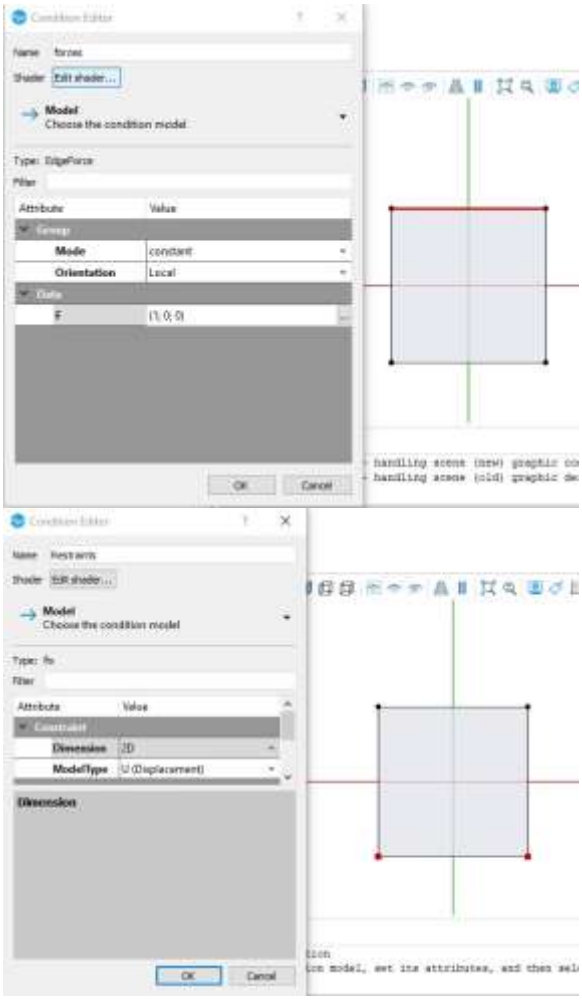

Figure 1.15. Screenshot of Boundary conditions in STKO software (ASDEA software, 2018)

To define where the analysis is going to save, there is the option of *analysis steps*. All the previous steps can be observed in the following items (fig. 2.16).

Once the properties are defined, the next step is to create the mesh in the mesh tab with the option *global edge seed* (fig. 2.17). The type of this option is set on uniform by size of 2. In addition, the set mesh control of the quadrilateral needs to be at a *structured* algorithm, a topology of *quad* and *linear* order. It is important to remember to assign all the properties to the quad by dragging and set the element with them. The last step of the pre-processor is to build the mesh (fig. 2.18).

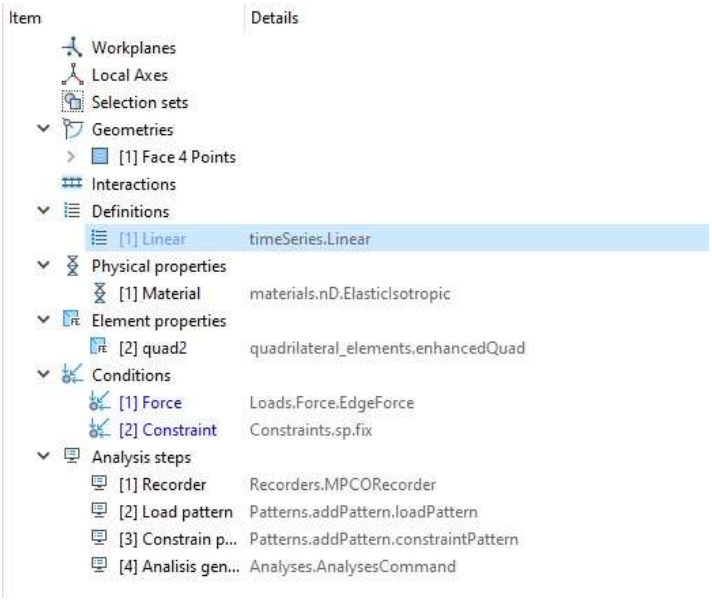

Figure 1.16. Screenshot of Items in STKO software (ASDEA software, 2018)

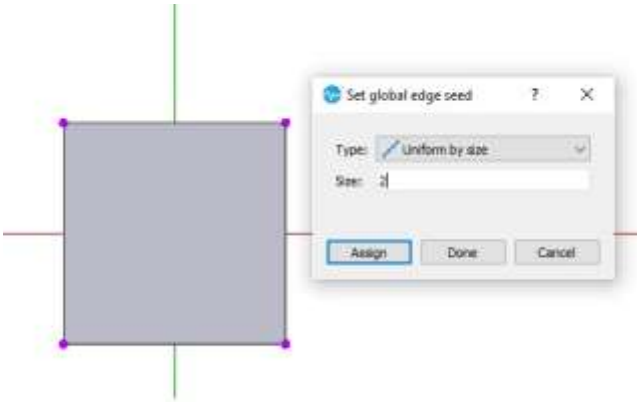

Figure 1.17. Screenshot of Set global edge seed in STKO software (ASDEA software, 2018)

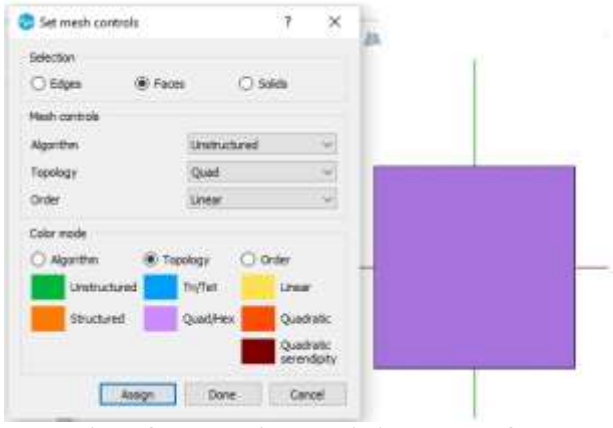

Figure 1.18. Screenshot of Set mesh controls in STKO software (ASDEA software, 2018)

The results of post-processor in STKO program (ASDEA Software, 2018)are included in fig. 2.19 for the strains and in fig. 2.20 for the displacements:

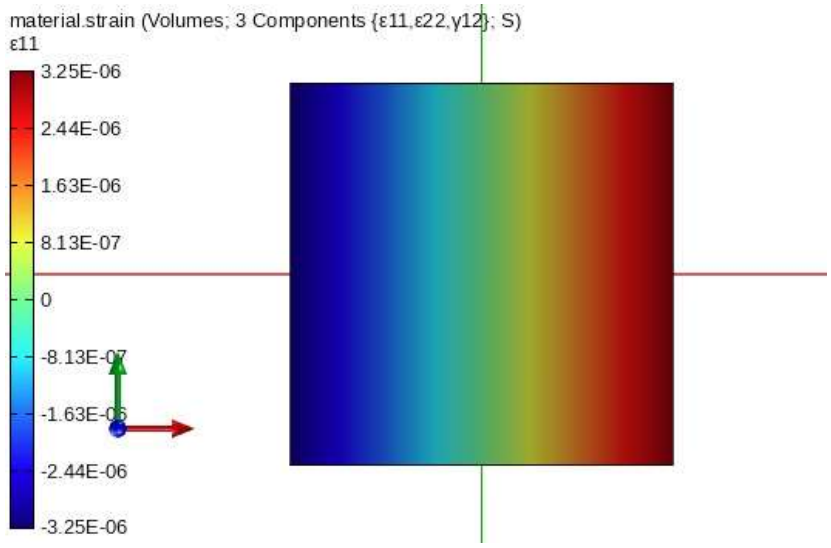

Figure 1.19. Strains results in STKO software (ASDEA software, 2018)

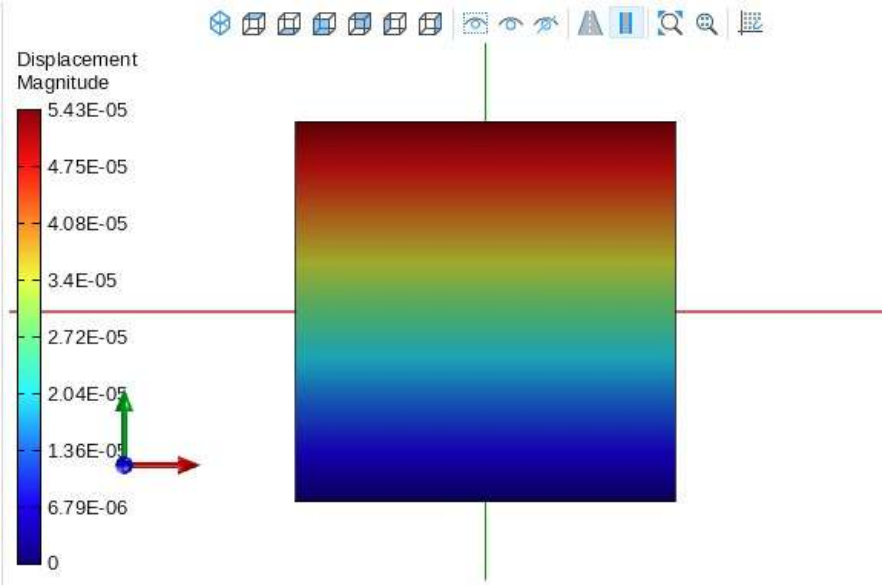

Figure 1.20. Screenshot of Displacement results in STKO software (ASDEA software, 2018)

I.VI Convergence analysis

Obviously, this software can be employed for problems which require a set of elements, *i.e.*, meshes. For this purpose, a convergence of the Cook's membrane problem (Cook, 1974) is performed. The geometric characteristics of the test describe a trapezoidal plate with a line of 44 mm on the left side and another of 16 mm on the right one. These two edges

form a slope between their upper vertices 16 mm above the top of the left side. To join all the points to form a trapezoid, two parallel lines are traced (Simo & F. Armero, 1992) (fig. 2.21).

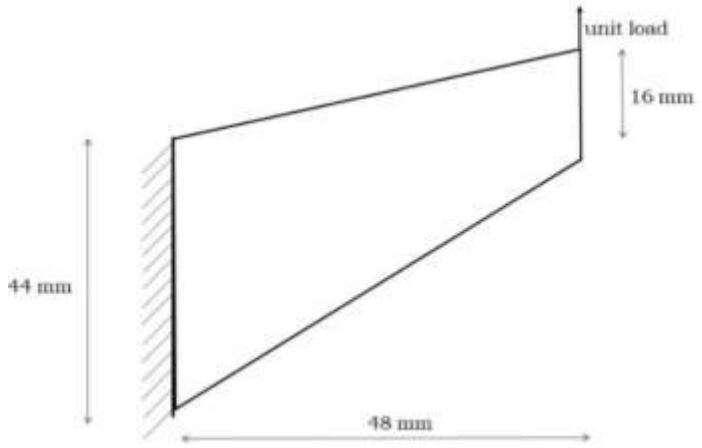

Figure 1.21. Cook's Membrane Geometry

As for the load, a unit edge load is applied on the right-hand side, and it has boundary conditions that fix the x-y plane faces on the left-hand side. A thickness of 1 mm is assumed to ensure a plane stress problem. Also, a Young's Modulus of 1000 MPa and a Poisson ratio of 0.2 are considered.

Once the geometry and properties are assigned in the STKO program (ASDEA Software, 2018), the convergence problem leads to dividing the membrane multiple times into 4 elements per each analysis. This describes an increasingly refined mesh of 2, 4, 8, 16 and 32 elements on the left side where the load is applied (fig. 2.22).

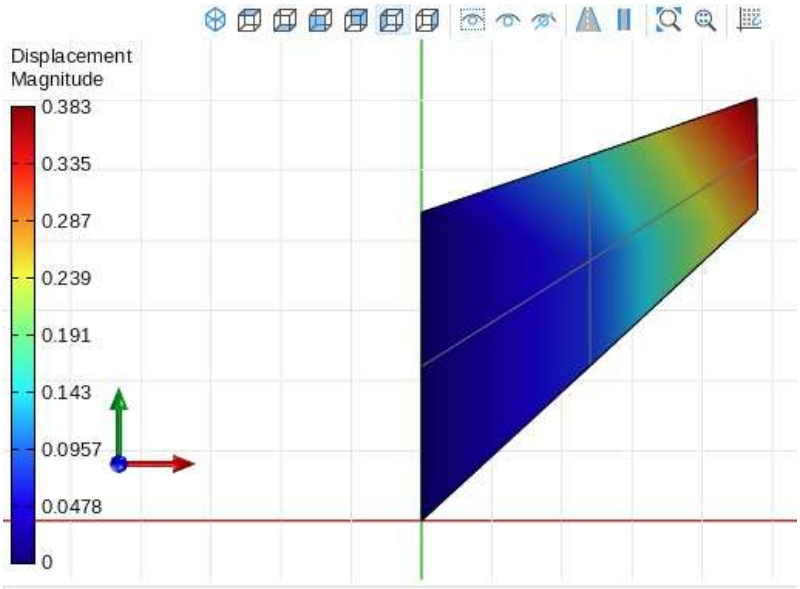

Figure 1.22. Screenshot of Cook's Membrane results for 4-element analysis in STKO software (ASDEA software, 2018)

All the results that were studied in the STKO postprocessor were plotted in terms of displacement in the highest point of the membrane. Once the results were extracted, several displacement elements were plotted. The plot of fig. 2.23 was obtained by increasing the numbers of elements in the membrane, where as mesh was finer, the closer it was to the analytical displacement result.

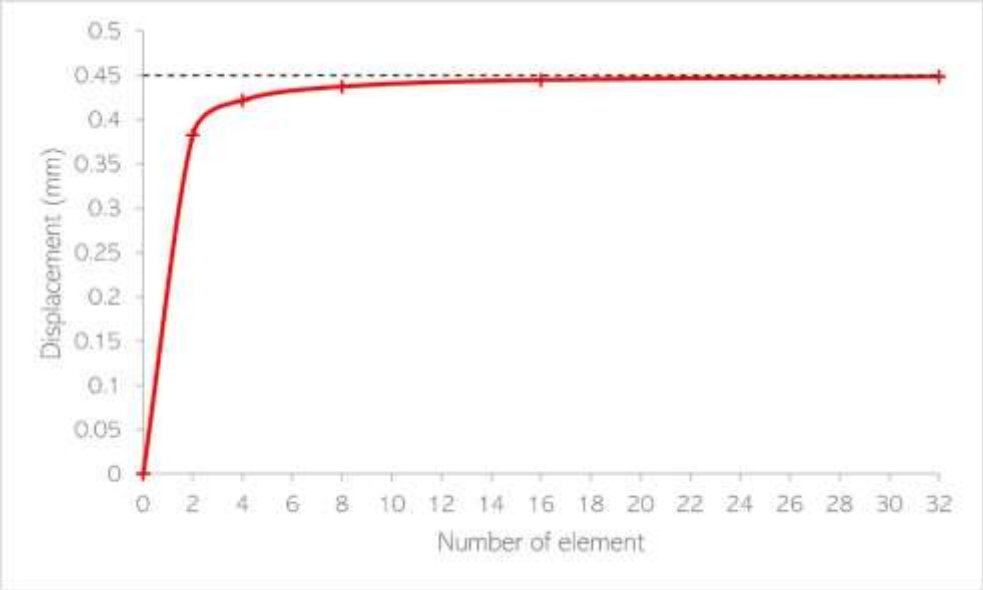

Figure 1.23. Number of elements-displacement graphic.

I.VII Overview of non-linear FEM analysis

Plasticity is the property of materials where permanent strains appear by a set of applied forces associated with an irrecoverable way of acting of the study object. Mechanical rheological models are a useful tool to have a graphic representation of the physical mechanism of stress-strain curve that is subjected to tension, and these can describe both an elastic phase and a plastic one. The main feature for an elastic material is the linear proportionality between stress and strain as the body is loaded or unloaded where the relation of these two properties is represented by Young's Modulus (E), (Olivella, 2000).

For an elastoplastic behaviour there is not uniqueness in the relation of stress and strain. The same quantity of strain can come for an infinite different amount of strain which also depends on the loading history. In addition, a non-linear model is expressed when the material suffers plastic

deformations. Moreover, these deformations can be directly proportional to the hardness of the material (Olivella, 2000).

The material needs to be tested in the plastic and elastic boundaries to design the element based in the estimation of collapse loads, taking into consideration the most economical one, through the available ductility of the material (Olivella, 2000).

The non-linear part of an elastoplastic formulation is normally associated with qualitative characteristics of the crack problems. The object of the crack theory is to stablish equilibrium to the body after damage has arrived, submitting to the body through a considerable quantity of finite strains. Summarizing the above, the material can be brittle but can resist before reaching the point of damage. In addition, cracks can be considered as discontinued surfaces (Olivella, 2000).

Moreover, when a system load appears into the body, the crack theory is formulated finding the values of stress and strain for crack situated in an initial position. Acting strains of the problem need to be finite, even so, if the initial location of the crack is not given a finite strain is assigned to be sure that the material is going to suffer damage (Olivella, 2000).

Chapter II
Sequentially Linear Analysis

II.I Introduction

Sequentially Linear Analysis (SLA) is a procedure, proposed by Rots et al. (2008), based on the performance of a series of linear finite-element analysis of structures in which the stiffness of certain element is decreased by the degradation of the material. This SLA procedure leads to a representation of the non-linear behaviour of structures of quasi-fragile materials such as masonry or concrete. Accordingly, SLA is an iterative aimed to acquire an approximation of the non-linear behaviour of the structures in terms of load-displacement curves and damage localization.

In order to approximate the non-linear behaviour of structures two type of analysis, among others, can be used, either a non-linear analysis employing constitutive models or a SLA employing saw-tooth softening laws. Through the years, the FEM has been improved with the main objective of obtaining an accurate numerical approximation of the non-linear behaviour of structures, but frequently real behaviour of structures have local peaks, snapbacks and valleys associated with brittle cracking (Rots et al., 2008).

According to the SLA method, bending diagram with negative slopes can be replaced with a saw-tooth model with positive slope inducing a material crack on a specific place (Rots et al., 2008), known as the critical elements, to make that happen SLA is applied with the main objective of reducing strength and stiffness of the critical elements of the mesh trying to give the closest approximation of the tension behaviour of quasi-brittle materials as concrete or masonry. The comparison between iterative responses and SLA can be interpreted with space and crack depth(Rots et al., 2008).

II.II Procedure description

In furtherance to avoid iterations of the Newton-Raphson method, it is sought to obtain a local brittle snap-back type response through Rots and Invernizzi (2008) SLA procedure.

By means of using the saw-tooth softening approach of a mechanical problems in terms of a strain-stress curve, a first critical element is chosen to give a secant restart made from the origin. Subsequently, the following assumptions are used to describe the procedure through the following algorithm by reducing stiffness (Rots et al., 2008):

1. The mesh must be created. All the elements in the mesh must be quadrilateral.
2. Assign where is going to be the specific area in which the damage is allowed.
3. Apply an external unit load.
4. Perform a linear-elastic analysis.
5. Select the critical element which is the one with the highest level of the principal stress.
6. Calculate the reduced modulus of elasticity for the current critical element (eq. 2.1):

$$E = \frac{E_{i-1}}{a} \tag{3.1}$$

   Here, a is a parameter that the user chooses according to the number of teeth.
7. Calculate the scale factor λ through eq. 2.2:

$$\lambda = \frac{f_t}{\sigma_t} \tag{3.2}$$

   Here f_t is the current tensile strength and σ_t is the principal tensile stress of the critical element.
8. Through multiplying the scale factor and the unit load previously applied in step 2; the critical global load is obtained.
9. Reduce the stiffness and strength, *i.e.,* Young's modulus E and tensile strength ft of the critical element, according to a saw-tooth tensile softening described above.
10. Through the repetition of step six to ten the method identifies a new critical element and so as the values of Young's modulus and tensile strength until the approximation is accomplished (fig. 2.1).

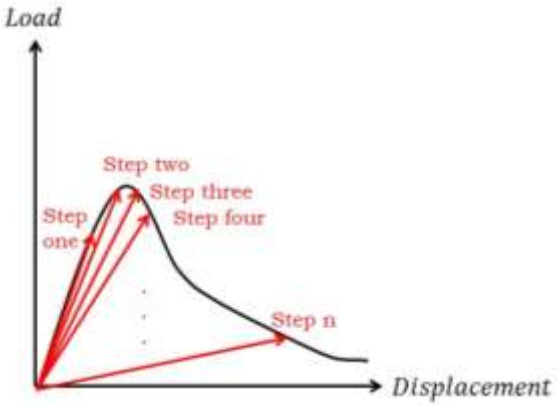

Figure 2.2. SLA procedure.

The softening diagram is formed by Young's modulus and the tensile strength, among others. The area underneath the diagram represents the fracture energy divided, G_f, by the crack width, h, which can be considered as a discretized parameter associated with the geometry of the finite element (Rots et al., 2008).

The procedure of a smeared cracking can be generated by a localized crack over a continuum stripe of finite elements with a crack opening, w, which is repeated several times to form a certain width, h. This width has influence in the mesh size through the tensile linear softening, although this parameter is not enough to define the mesh density (Rots et al., 2008). Furthermore, the ultimate strength, ϵ_u, depends on the cracking strip with, h, width. And it can be calculated thought equation 3.3:

$$\epsilon_u = \frac{2\,G_f}{f_t h} \tag{3.3}$$

where the reduced tensile strength, f_t, can be obtained as (eq. 3.4):

$$f_t = \epsilon_u E_i \left(\frac{D}{E_i + D}\right) \tag{3.4}$$

And D, represent the tangent to the stress strain softening diagram (eq. 3.5):

$$D = \frac{f_t}{\epsilon_u - \left(\frac{f_t}{E}\right)} \tag{3.5}$$

On the other hand, when the saw tooth diagram is being built by the SLA method, the regularization procedure helps to fix the underestimated loads and displacements. To begin with, a new expression (eq. 3.6) is provided to

determine the current area, A, bellowing the curve. Later, it is updated the tensile strength, the ultimate strain, or either both in contemplation of keeping the invariant energy dissipated, in other words, the newly updated area, $A*$, of the constitutive law becomes invariant and is equal to (Rots, 2018):

$$A* = \frac{G_f}{h} \tag{3.6}$$

In addition, the tensile strength, and the ultimate strain are multiplied by a numerical factor known as, k, (eq. 3.7):

$$k = \sqrt{\frac{\frac{G_f}{h}}{\sum_{i=0}^{N-1} \frac{1}{2} \frac{f_t^2}{E_i} b_i}} \tag{3.7}$$

Where, b_i, varies depending on the approximation method in the saw-tooth diagram. The following figure (fig. 3.2) represents the regularization procedure.

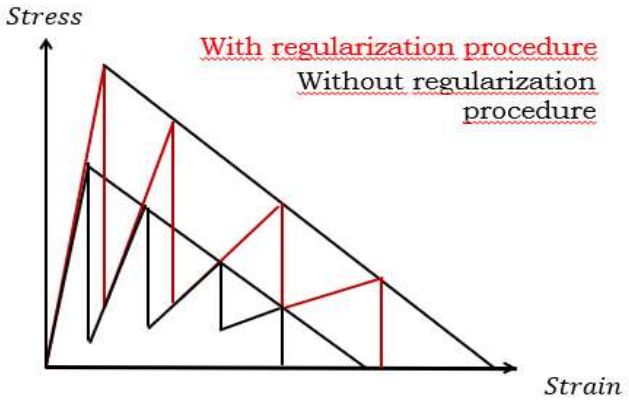

Figure 2.2. SLA with and without regularization procedure

II.III Implementation using a stabilization procedure for reduced integration

In the original proposal for the SLA procedure, RI techniques are normally used in the on the elements where the damage is expected to occur. In terms of the SLA method, every element belonging to the branch of softening can not be used as the weakest element a lot of times during the analysis. Furthermore, when the Young's Modulus approaches to zero, the stops in order to avoid numerical issues.

In terms to determine the critical load where the element will suffer damage, the a parameter would help to determine it. On the other hand, the fracture energy is represented by the area down the curve of strain-stress diagram results.

II.IV Calibration example

In the following lines, an example is included in order to describe the SLA procedure. This example consists on a concrete notched beam that was analyzed in the investigation of Rots (Rots et al., 2008) and was also evaluated by Amezcua ((Amezcua, 2022), the main objective of this section is to obtain the same results to prove that the analysis was correctly applied.

The mechanical material properties for the material are the following:

- Young's modulus $E = 38000\ MPa$
- Poisson's ratio $\nu = 0.20$
- Initial tensile strength $f_y = 3\ MPa$
- Fracture energy $G_f = 0.06\ \frac{N}{mm}$
- An a parameter of 4, 2 and 1.4142 for a five, ten and twenty teeth, respectively
- Total depth of the beam of $t = 50mm$

Where the geometry of the example, is described in the following fig. 2.3:

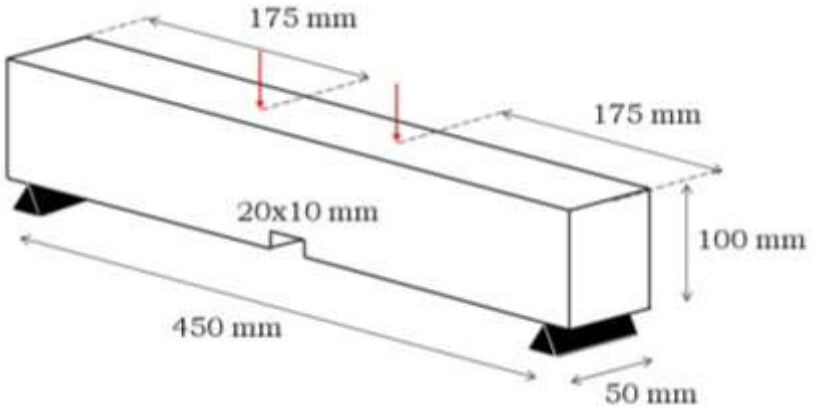

Figure 2.3 Notched beam's Geometry.

For this example, are considered five, ten and twenty teeth with and without the regularization procedure to represent the behaviour in terms of load and displacement. Moreover, quadrilateral elements were implemented in the whole structure with three different width sizes, in the first place, dividing with 35 rectangles from the sides of the beam to 175 mm thought the center and a load applied at the top where this mesh size ends. The selected crack path can be symbolized as the red strip in the following fig. 3.4.

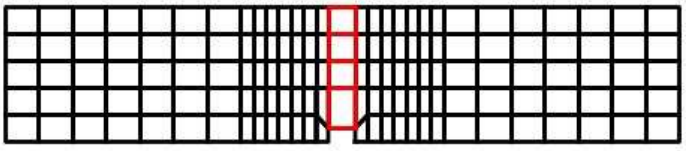

Figure 2.4 Proposed mesh

The results of the softening tension curve for each number of teeth are showed in the following figures. Here it can be observed that every tooth is represented for a spike. These results are comparable with the graphics of other authors as Amezcua (Amezcua, 2022) and Rots (Rots et al., 2008).

II.IV.I Without regularization procedure.

As it might be seen in the consequent figs. 3.5 to 3.7, the ten teeth graphics are more difficult to detect for the irregular form of the peaks. Nevertheless, it can be observed that a more accurate approximation to reality is stablished which proves that with a greater number or teeth the algorithm establishes better results. However, all the graphics are under the results of the real problem at least half of the steps for the SLA procedure.

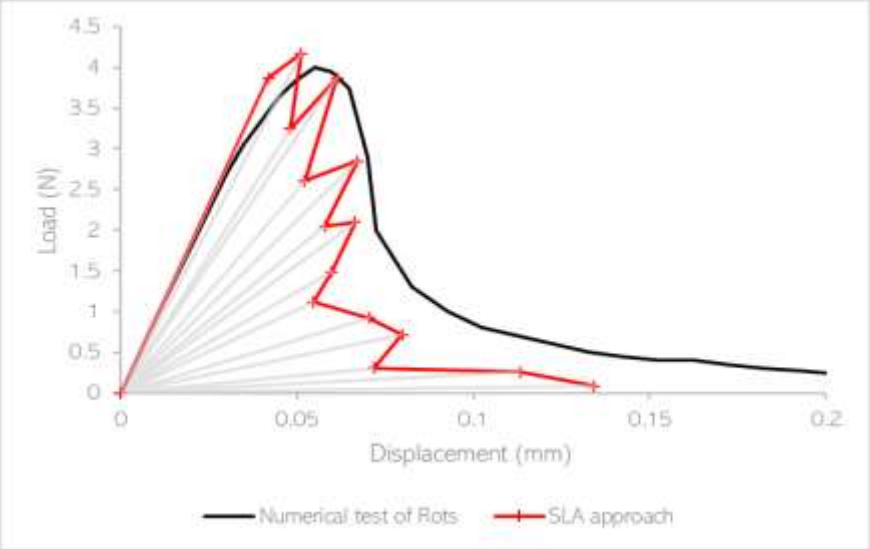

Figure 2.5. Load-displacement diagram for an SLA with five teeth.

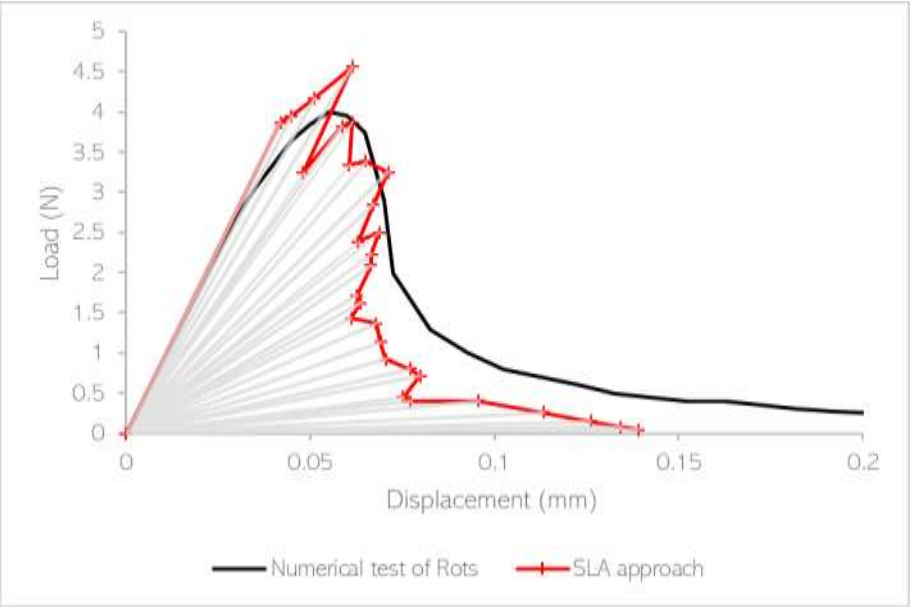

Figure 2.6. Load-displacement diagram for an SLA with ten teeth.

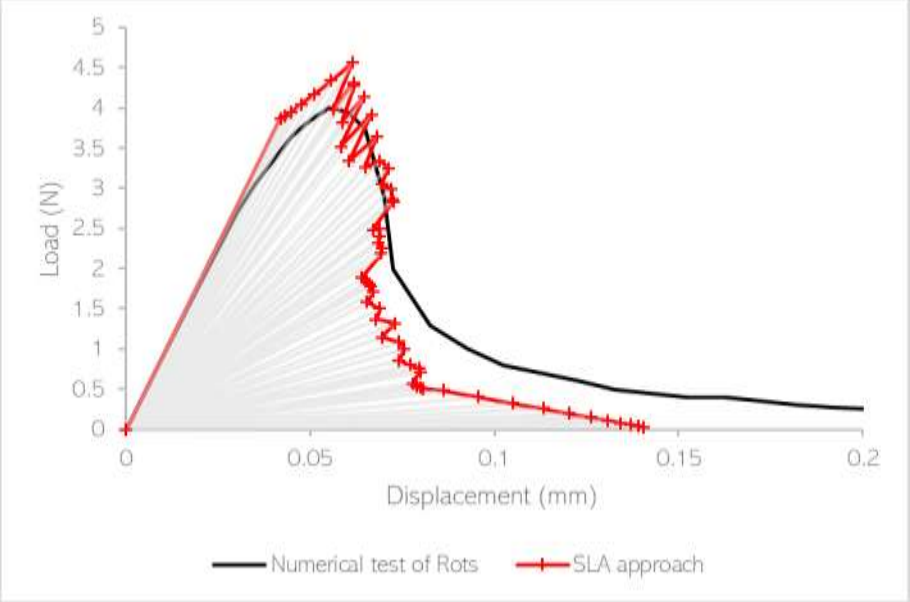

Figure 2.7. Load-displacement diagram for an SLA with twenty teeth.

II.IV.I With regularization procedure.

For the following figs. 3.8 3.10 the approximations mark subsequent peaks are plotted very closely to the numerical model. As can be observed, the

load-displacement results seem to be effective when the regularization procedure is applied in the SLA method.
As the previous example, the more teeth are considered, the closer the results.

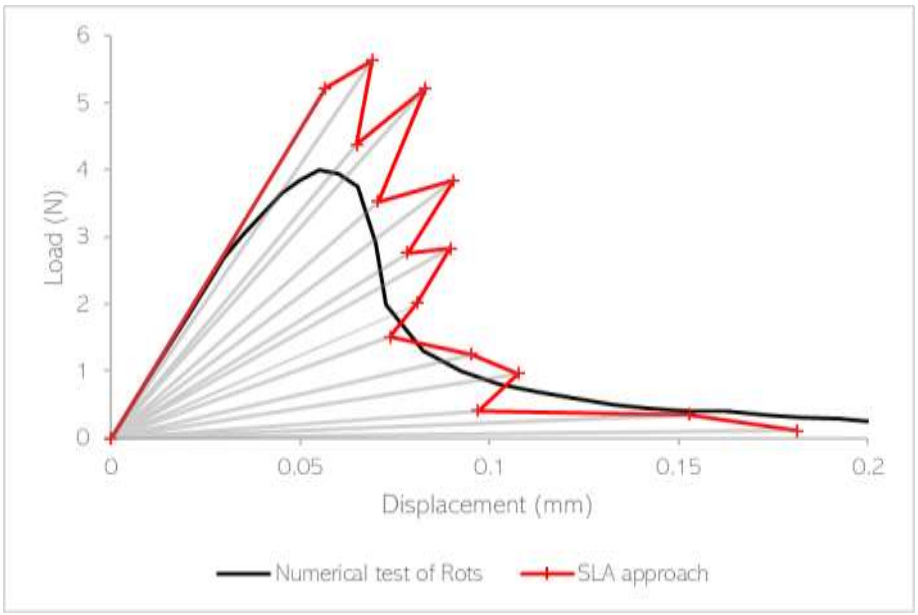

Figure 2.8. Load-displacement diagram for an SLA with five teeth with regularization procedure.

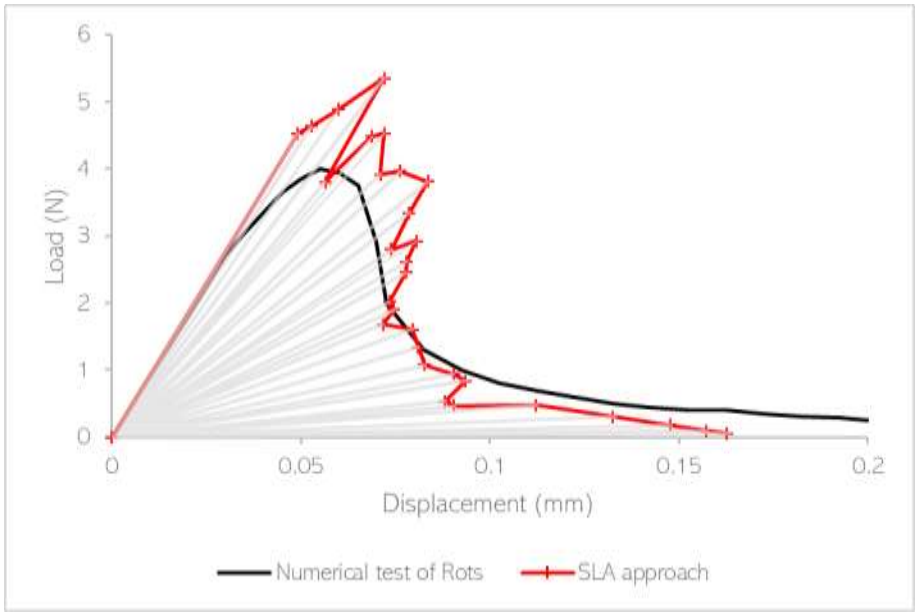

Figure 2.9. Load-displacement diagram for an SLA with ten teeth with regularization procedure.

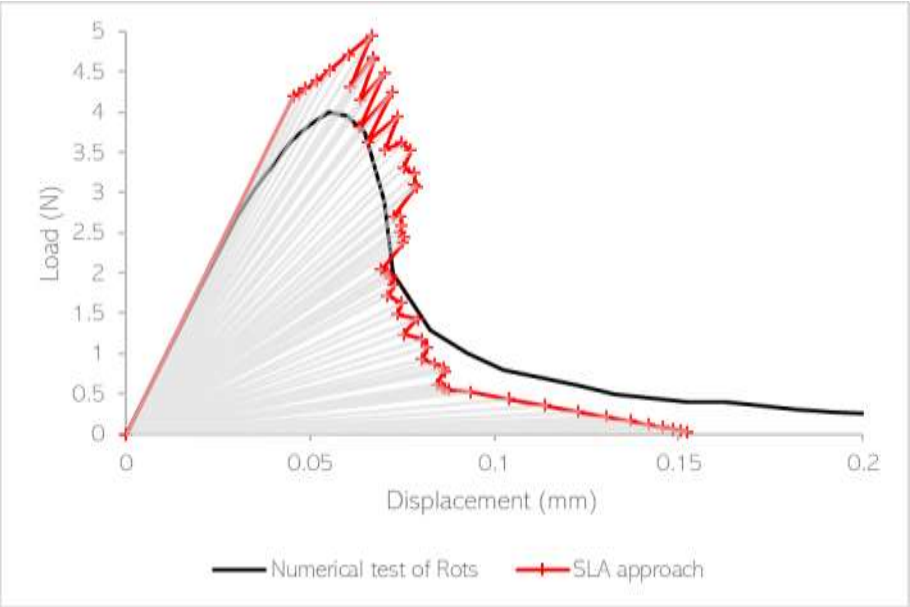

Figure 2.10. Load-displacement diagram for an SLA with twenty teeth with regularization procedure.

Chapter III
Application examples

III.I Introduction

To represent the previously described formulations, an analysis of a tension plate by using SLA as an alternative of non-linear analysis of structures was performed. The selected problem consists on a specimen that was tested by Van Vliet (Van Vliet, 2000) and studied by Retama (Retama, 2010). The SLA solution proposed in this chapter was studied by Rots (Rots et al., 2008) whose study described a method using SLA with saw-tooth softening.

The objective of this chapter is to compare the different scenarios obtained for the same problem of a tension plate. The study cases considered in this example include stabilized reduced integration and the regularization procedure, as well as combinations of their absence, giving a total of 4 per number of teeth.

Likewise, in the calculation of the new Young's modulus of the critical element, having different alpha values in the number of total steps in the repetition of runs at the time of obtaining the sawtooth diagram was considered in order to compare with a constant alpha analysis.

III.II Tension plate example

An example studied by Van Vliet (2000) was selected to obtain a numerical approximation of the test results obtained in the experiments carried out in the Technical University of Delft. The sample that was selected to be analyzed through the SLA procedure was the designated as "Type C"., Two of the three dimensions were considered to have a two-dimensional plane-stress problem. Therefore, the thickness of the concrete specimen is indicated as a constant magnitude and is referred as "t". The value of this thickness is 100 mm.

The geometry and the shape of the specimen were tested multiple times to determine the sections and their equivalences in function of the dimension "D" as is shown in fig. 4.1. The base length is determined by dimension "D"

which, for the type C, is considered as 200 mm. Moreover, the shape of the specimen is described as a concave plate that is anchored at its ends to a steel material. The radius of this specimen at its concave spaces is 145 mm.

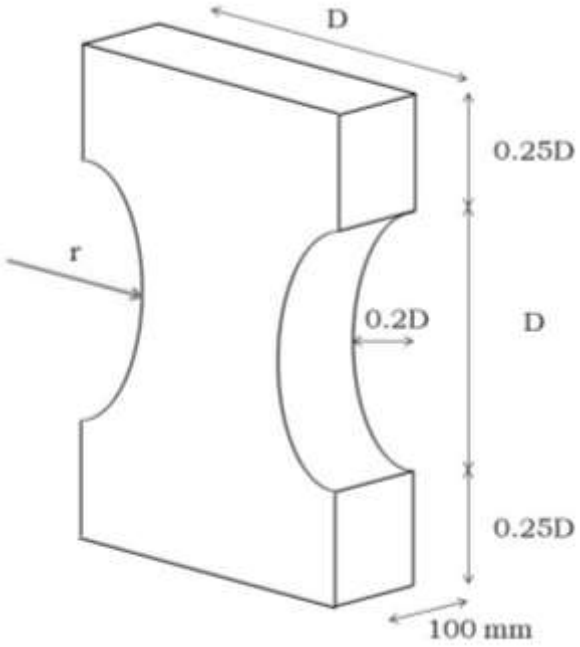

Figure 3.1. Plate's Geometry

These dimensions were taken from the Van Vliet's work (Van Vliet, 2000) in addition to the material properties and the boundary conditions which specify that the specimen is subject to limited conditions. Moreover, a prismatic sample was used to minimize shape effects in order to have the crack at the weakest zone of the specimen. Therefore, the initial crack must be further away the fixed constraints. As shown in the fig. 4.1, the vertical dimensions are dependent of "D" where those of the ends are 0.25 times D.

The dimension of the center is also given by D. The depth of the radius where the force is applied 0.2 times D from the limits of the figure to the center.

Type C specimen had free rotations in two orthogonal directions and two steel hinges were used to apply a uniform load, this steel plate functions as a connection between the specimen and the experimental set up. Despite the differences of the Young Modulus or the Poisson's Ratio, stress concentrations cause material failure near to the glue layer. To avoid this situation, the cross-section is increased, and the boundary stresses are reduced. This shape description was designated by Van Vliet to find the best option for performing a uniaxial tensile test on a plate (fig. 4.2).

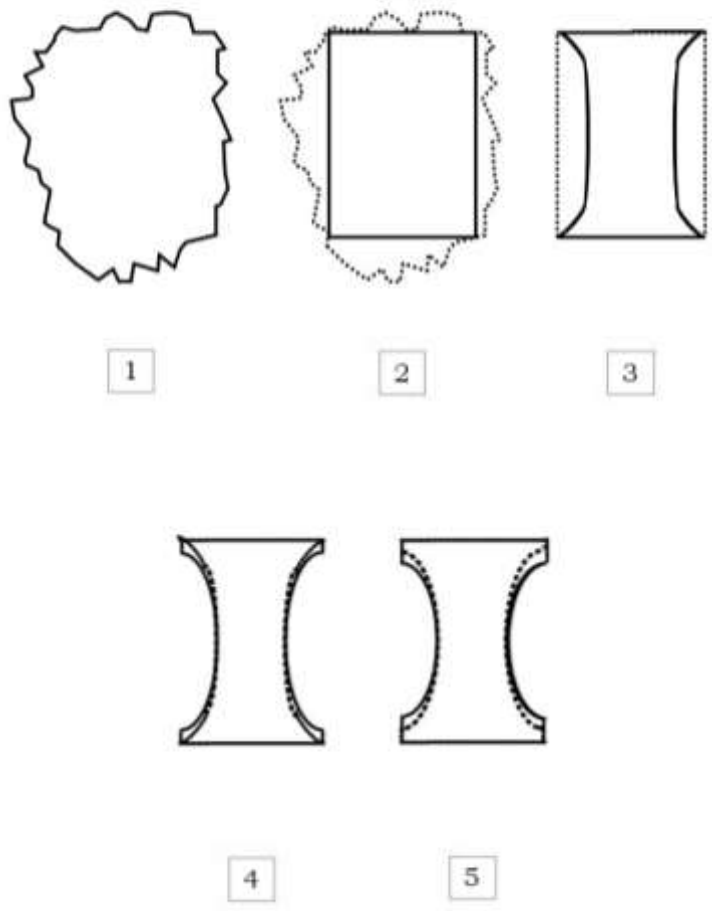

Figure 3.2 Design of the specimen shape for the size effect test (Van Vliet, 2000)

The concrete and steel plates were joined by four fixed lower and upper hinges at 320 mm joints, several bolts of 2x2 and 20x2 steel angles, which allowed free rotation. The load plates and hinges were glued to the concrete specimens.

Regarding the loads, a "P" load was applied with an eccentricity between the axis of symmetry through a hydraulic actuator and the point of application. This uniaxial tensile test was performed under control and the strains were measured by LVDTs (Linear Variable Displacement Transducer) at two points. The first stage consists on apply a small, constant load whose displacement for the control LVDTs could be measured. The second stage was to find the maximum deformation through a feedback signal known as the "MAX" control in the test report of Van Vliet. A total of 16 LVDTs were used at the first and second point of application. (fig. 3.3).

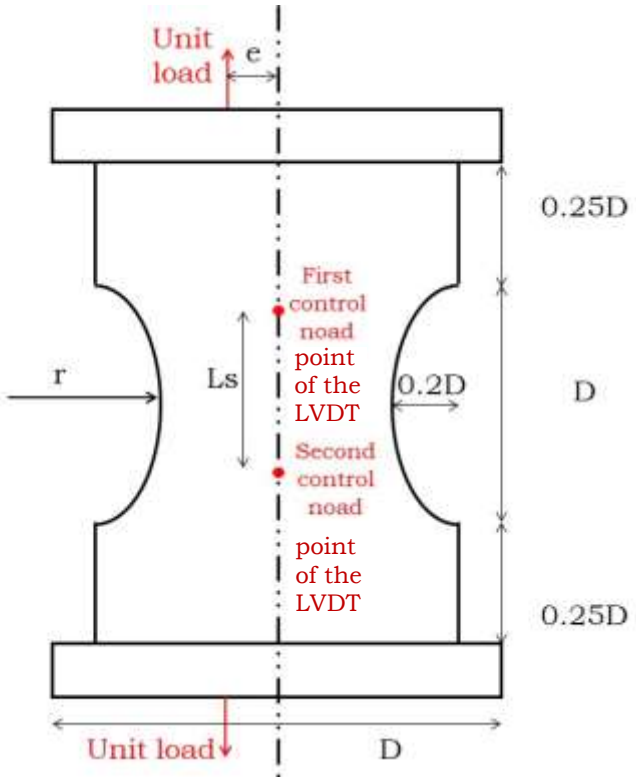

Figure 3.3. Study plate

The center of the concrete plate was the area where failure is expected to occur. To guarantee the tensile state of stress in the cross-section, the eccentricity of the applied load was calculated as $e = \frac{D}{50}$. The two reference points where the deformation was measured were over the middle cross-section, which were separated by a magnitude "Ls". The calculation of this magnitude could be obtained by multiplying 0.6 by D (Retama, 2010).

To review the final dimensions of the Type C specimen; a length of 200 mm, radius of 145 mm, depth of 100 m, load eccentricity of about 4 mm, distance from the reference points of 120 mm, the height of the concrete bases of the plate above and below are 50 mm and the distance of the arcs where the radius is applied are 40 mm (fig. 4.4).

The combination of all these geometry and material characteristics were classified as 05C04N30 in the experiment report (Van Vliet, 2000) where the digit 05 means the casting number, C is the letter to represent the type of test piece, 04 is the number in millimetres of the eccentricity, N is the material tested (concrete) and the 30 number was to indicate the unique sequential number.

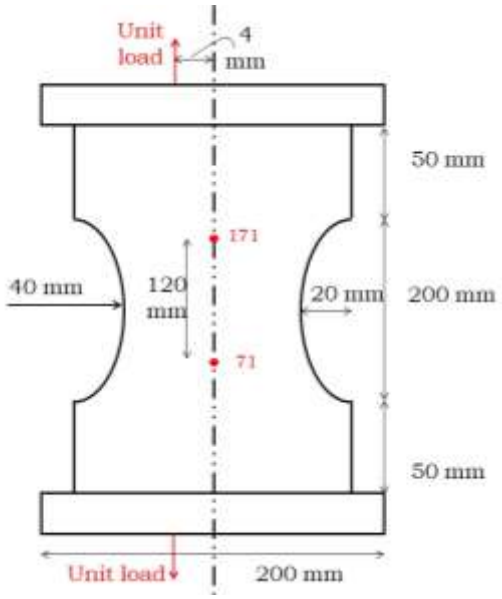

Figure 3.4. Type C specimen.

III.III Description of the numerical model

Following the previous procedure of discretizing the plate in finite quadrilateral elements, a mesh was created to obtain an approximation of the physical results obtained by Van Vliet (2000). To design a suitable mesh of the problem, two different software were used: AutoCAD and GiD. The first CAD software was only used to draw the plate and mesh geometry (fig. 4.5) where the eccentricity needs a diagonal line to apply the load to have the right proportion of the quadrilateral elements throughout the concrete specimen.

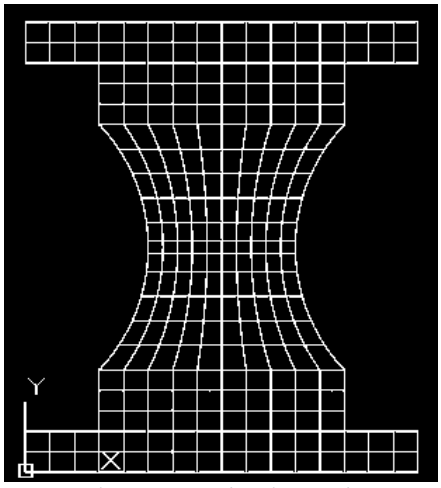

Figure 3.5. Plate's mesh.

The second software was used to generate the mesh, *i.e.*, the nodes, elements, restraints and loads, so that the program for performing the SLA procedure (Amezcua, 2023) could read it.

To read all the elements, a GiD file needs to be created. The following algorithm works to describe the exact usage of the GiD software:

1. To create nodes between divisions, choose the *geometry* menu, go to *Edit* and *Intersect*, click the line option, and select the entire shape. Press *OK*. Then go back to the *geometry* menu and build a *NURBS* surface with the create option. Select *Automatic* and type the number 4.

2. To create the mesh from the read file, go to the *mesh* menu and select the *quadrilateral element type*, then select *generate mesh* (Fig. 4.6).

3. The last step is to export the mesh register in the *file* menu.

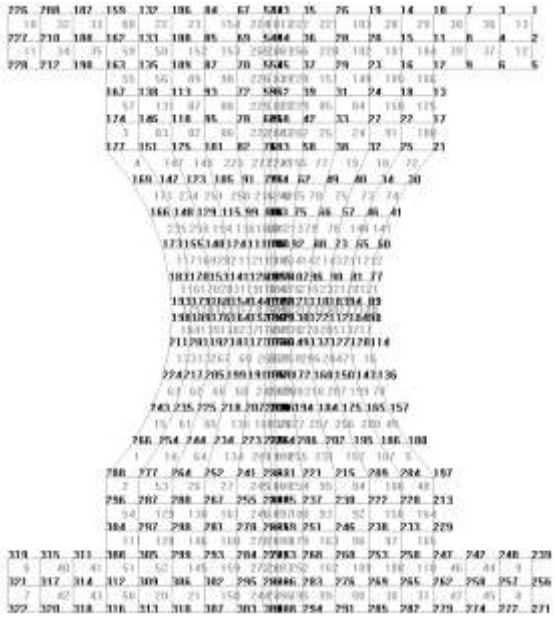

Figure 3.6. Plate's mesh in Gid.

As a result, the GiD Software displays a numbered mesh file that the SLA program reads as a discretized specimen to work by the FEM (fig. 4.7). To run the program, it is necessary to enter the material properties that were used in the Van Vliet's test. To begin with, the magnitude of Elastic modulus $E = 39800\ Pa$, a Poisson ratio $\nu = 0.2$, tensile strength

$\sigma_{t0} = 2.57MPa$ and fracture energy $G = 0.1219\frac{N}{mm}$. The other parameters to be entered due to SLA depend on the study model.

In terms of the method, there are a series of elements that must have a compressive behavior in all uniaxial tensile tests because the unitary load stretches the specimen with an eccentricity that makes the entire element rotate to its right side. This behavior will imply that the central elements of the plate are compressed a little and they will be considered as cracking elements of the material. According to the analysis and the results, only some test where the compression is going to be analyzed.

Regarding the crack, a crack band is located where the damaged area is already known, where the quadrilateral elements known as 48, 122, 169, 172, 210, 211, 213 and 229 make the crack pattern, such as seen in the fig. 4.7. Additionally, the FEM in these elements is applied with RI because, otherwise, four different values of principal stresses would be obtained as a result.

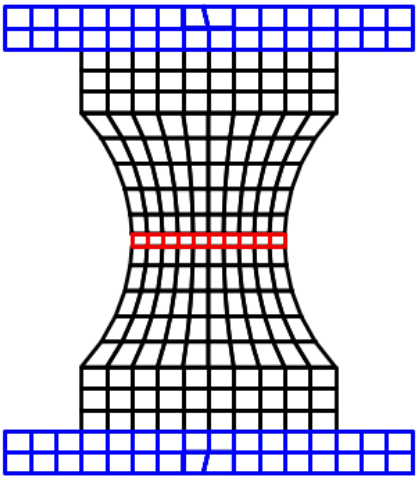

Figure 3.7. Mesh employed in the analysis

For the numerical approximations, two case studies will be shown. First, the a parameter was considered as a constant for each step of the SLA according to the liner softening saw-tooth law. Second, the a parameter varies following a multi-linear global softening law. These two cases are studied to compare the results for the plate test. Additionally, a regularization procedure and the SRI scheme are used for comparison purposes. The results presented in the next chapter are analyzed for 5, 10 and 20 teeth.

The load-displacement experimental results of the tension plate test (fig. 4.8) are included in Table 4.1:

Table 3.1. Tension test results

Van Vliet's Test	
Displacement (mm)	Load (N)
0.000	0
0.000	0.118
0.001	5.093
0.002	9.831
0.003	15.043
0.005	19.900
0.006	24.163
0.007	26.769
0.009	24.871
0.016	19.531
0.020	14.668
0.028	11.578
0.039	8.840
0.057	6.923
0.080	4.526
0.104	3.313
0.129	2.335
0.153	1.478
0.173	1.336
0.199	0.949

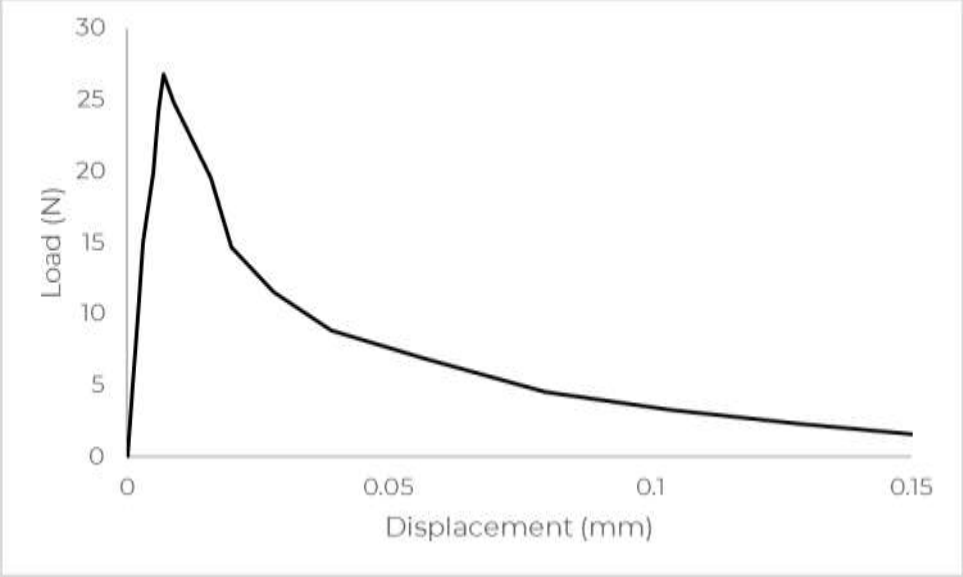

Figure 3.8. Experimental results for the plate

III.IV Results

A description of each considered case for the SLA is included in the following list.

Case 1. Without regularization procedure (RI-NR-n)
Case 2. With regularization procedure (RI-R-n)
Case 3. Stabilized reduced integration without regularization procedure (SRI-NR-n)
Case 4. Stabilized reduced integration with regularization procedure (SRI-R-n)

Here, n indicates the number of teeth considered in the analysis. Additionally, in a first stage, the four cases consider a as a constant for each step of the SLA with a different value for each type of analysis depending on the number of teeth and, in a next stage, a is considered variable for each third of the total steps. For this purpose, an implementation was added to the SLA program to calculate the reduced modulus of elasticity for the current critical element.

Displacement results were obtained at two different nodes of the mesh, numbered as node 171 and 71, where every displacement of the two points is added. For the other hand, load will be the same calculated for every step.

For the other hand, load will be the same calculated for every step. Once the results were obtained, the load-displacement diagrams were constructed. For the Case 1, for a 5, 10 and 20 teeth, *i.e.*, RI-NR-5, RI-NR-10 and RI-NR-20, the graphs are described by figs. 3.10 to 3.12 where the a parameter was considered as constant of 4, 2 and $\sqrt{2}$.

Also, the number of steps was determined and growing according to the number of teeth, for each case.

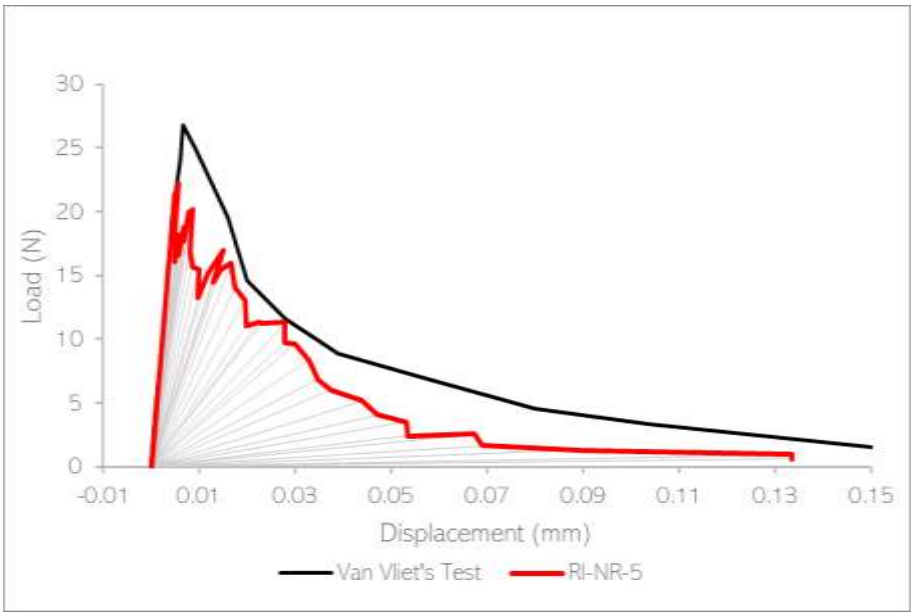

Figure 3.9. SLA results for case 1 (RI-NR-5)

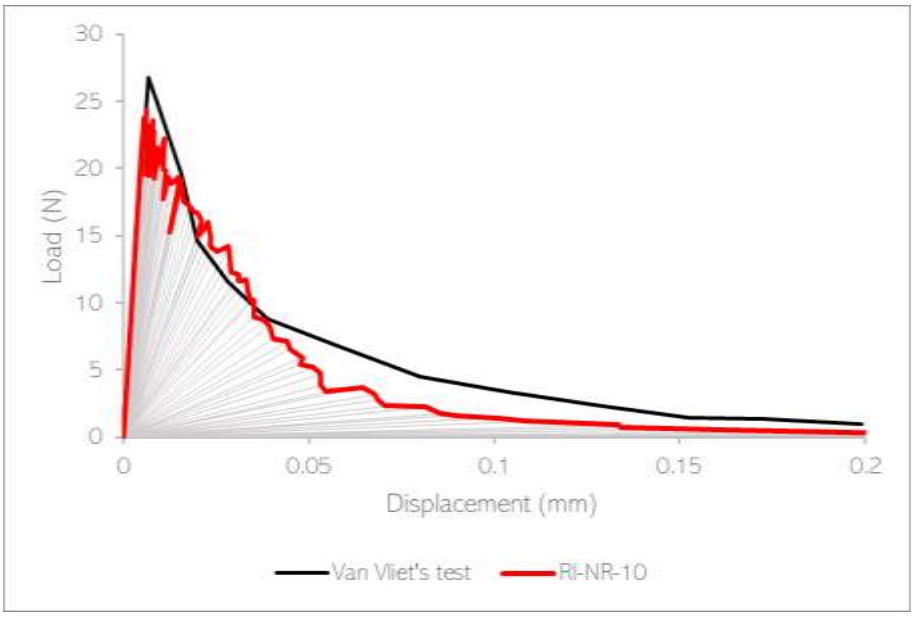

Figure 3.10. SLA results for case 1 (RI-NR-10)

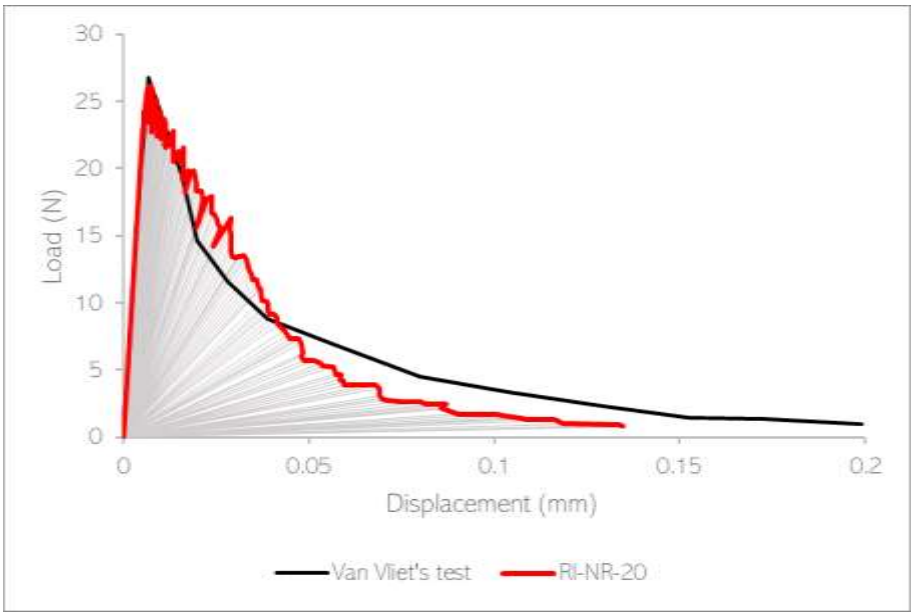

Figure 3.11 SLA results for case 1 (RI-NR-20)

The Case 2 is for an analysis performed with a regularization procedure that makes the diagram fixed for correcting the underestimated fracture energy. Depending on the analysis and the characteristics of the geometry and the case, the results obtained with SLA will represent that for the same displacements the plate resists more before suffering damage (figs. 3.13 to 3.15). The different a parameters were the same as the previous case of study.

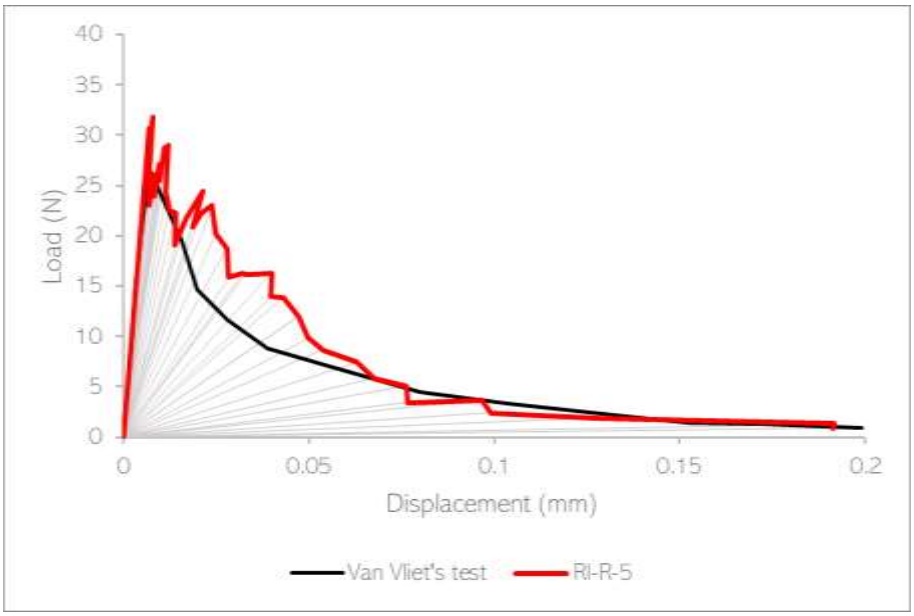

Figure 3.12 SLA results for case 2 (RI-R-5)

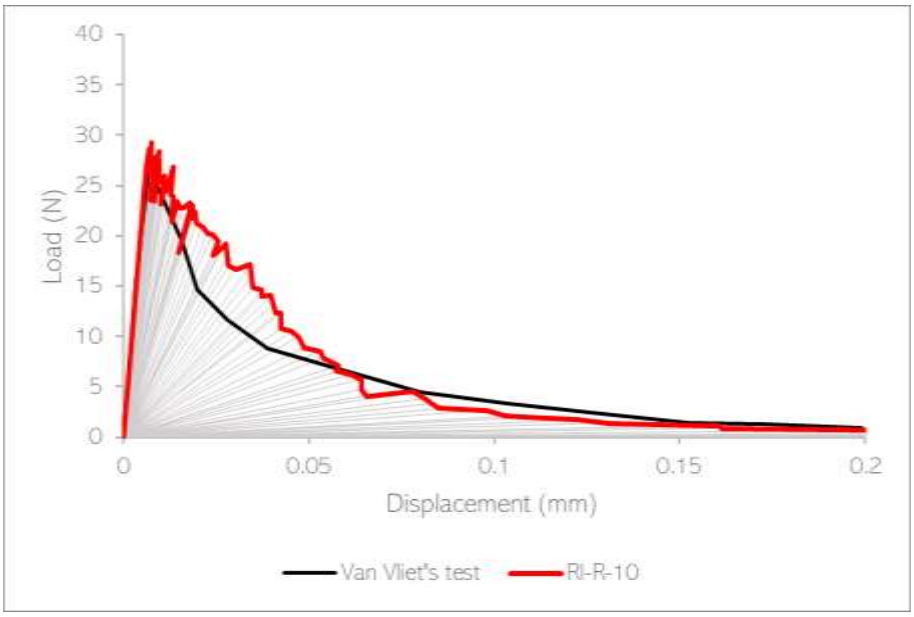

Figure 3.13 SLA results for case 2 (RI-R-10)

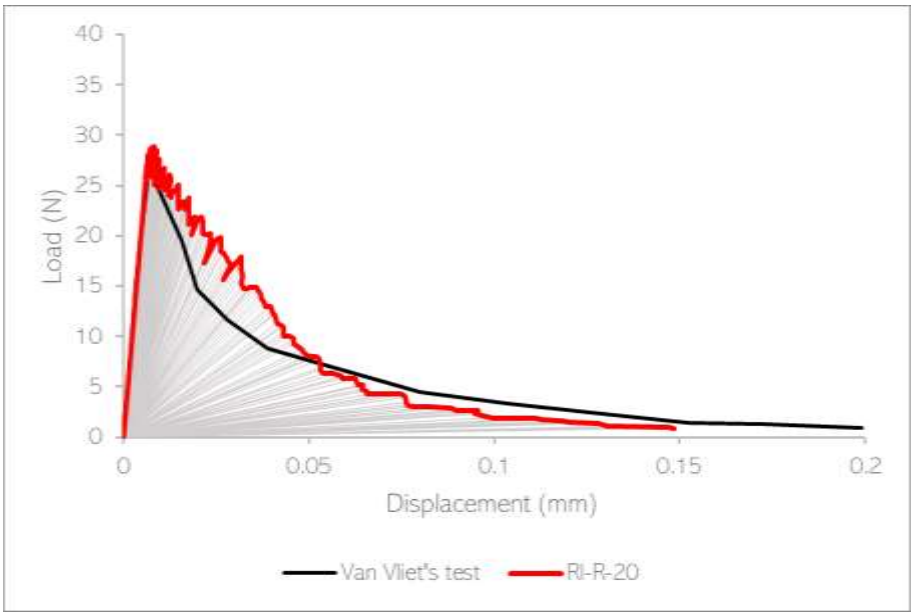

Figure 3.14 SLA results for case 2 (RI-R-20)

The Case 3 of study corresponds to the SRI, described in the chapter 2, without regularization procedure. The values of the parameter a were the same as the previous case (figs. 3.15 to 3.17).

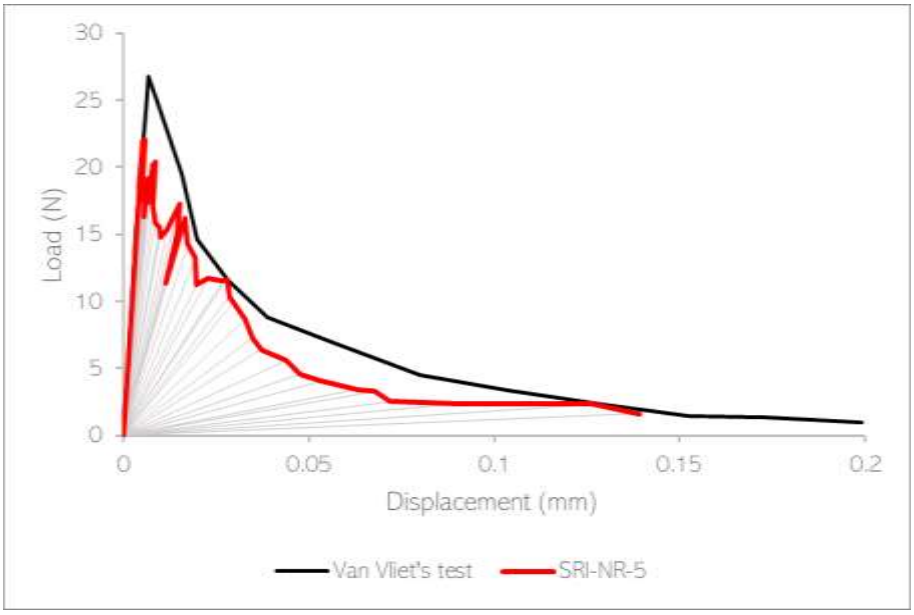

Figure 3.15 SLA results for case 3 (SRI-NR-5)

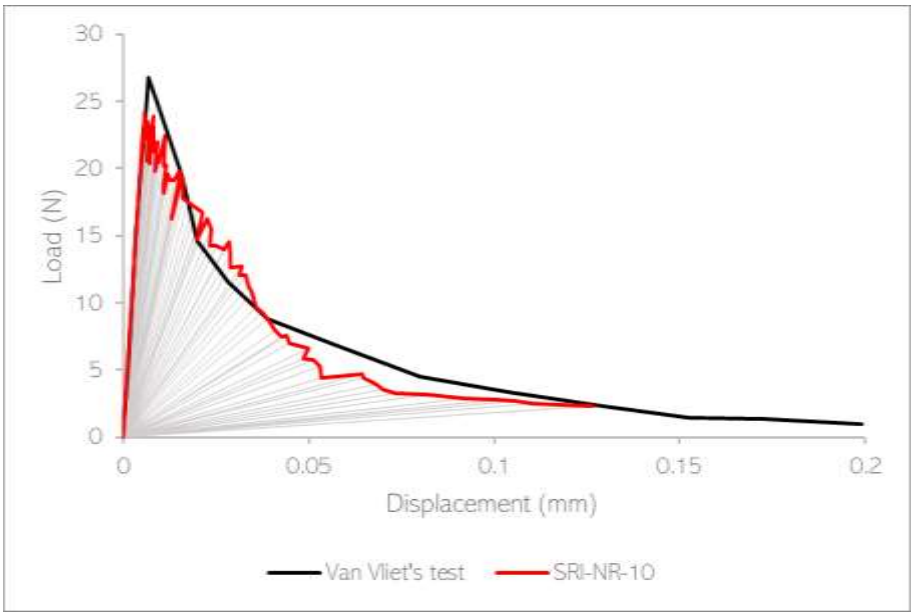

Figure 3.16 SLA results for case 3 (SRI-NR-10)

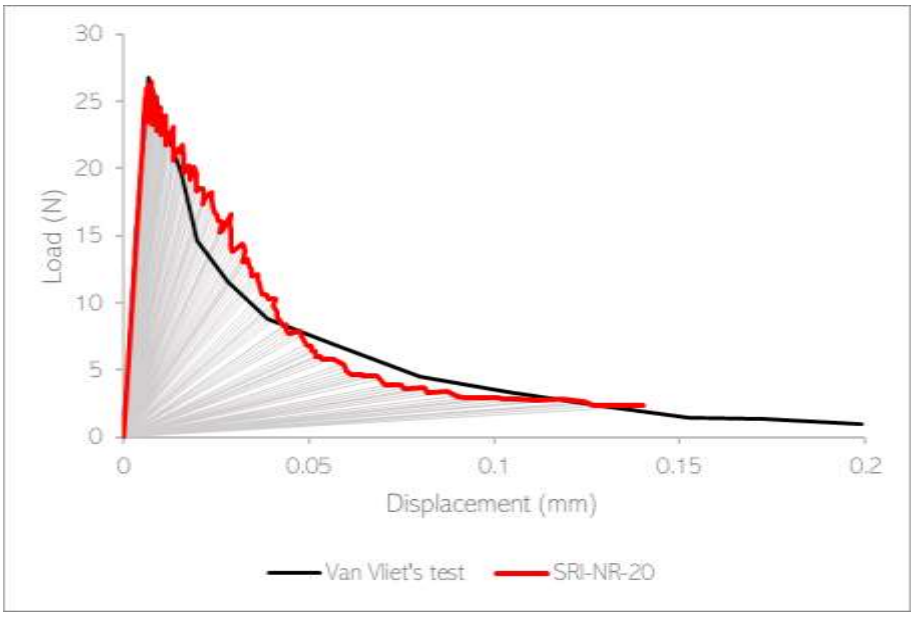

Figure 3.17 SLA results for case 3 (SRI-NR-20)

The Case 4 is considering SRI with a regularization procedure. Also, like the other case studies, the parameter a was the exact same as the last case of study (figs. 3.18 to 3.20).

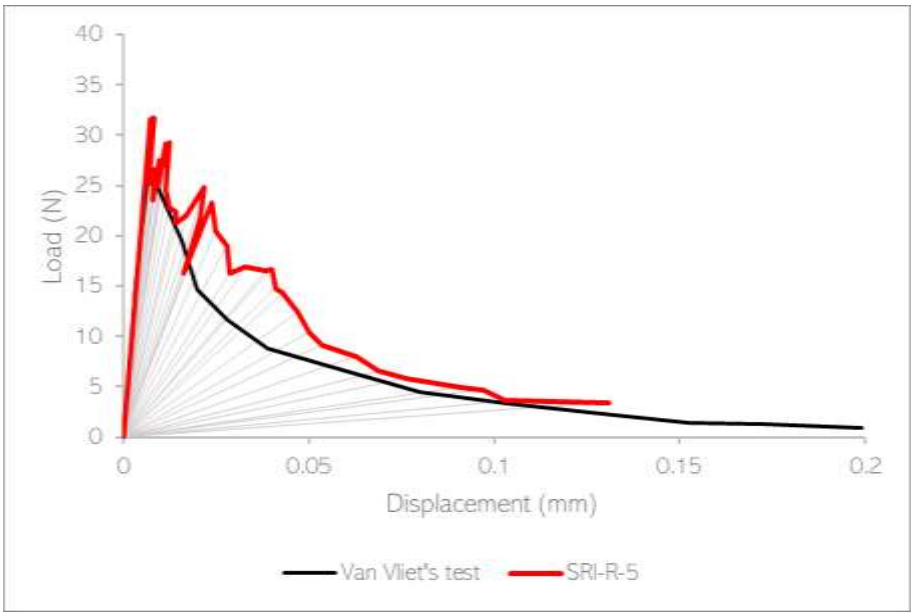

Figure 3.18 SLA results for case 4 (SRI-R-5)

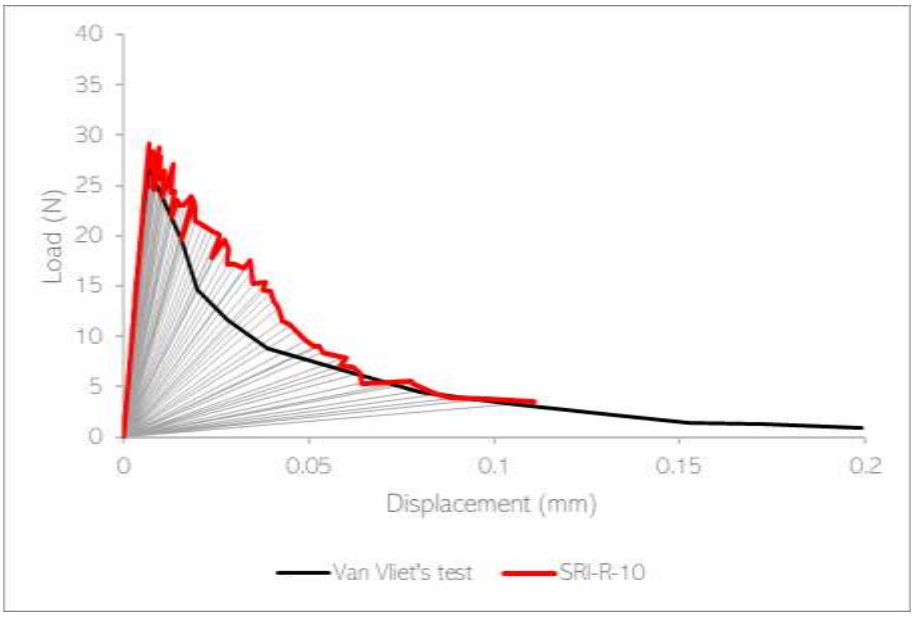

Figure 3.19 SLA results for case 4 (SRI-R-10)

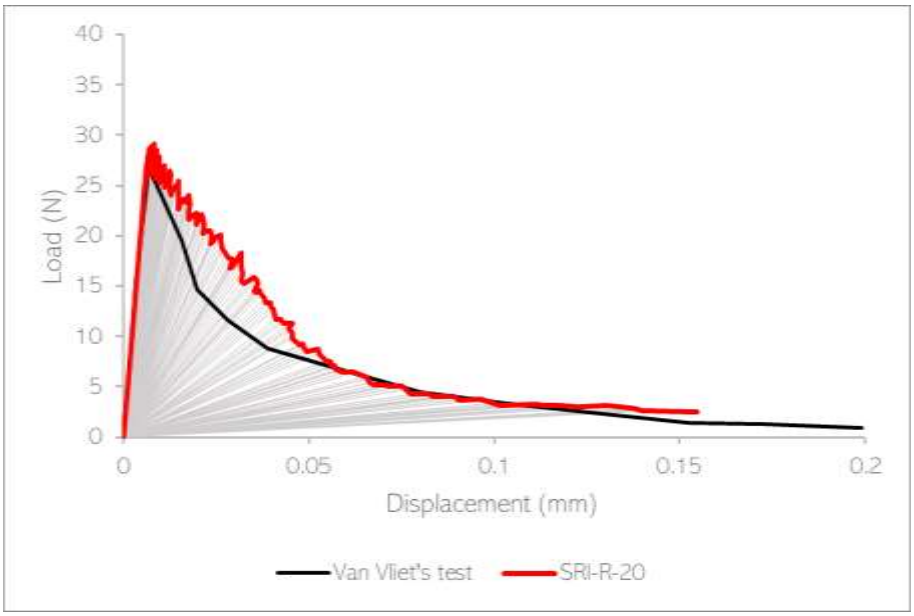

Figure 3.20. SLA results for case 4 (SRI-R-20).

As a result of comparing the graphics for all the cases, it can be noticed that the case of SRI-NR-20is the one with better results; nevertheless, by displacement 0.01(mm), the mechanical property of the critical element needs to be more reduced. To obtain the best approximation, a variable a parameter is going to be used (Table 3.2):

Table 3.2. Tension test

Step	a
0-60	1.4142
60-96	2
96-170	1.4142

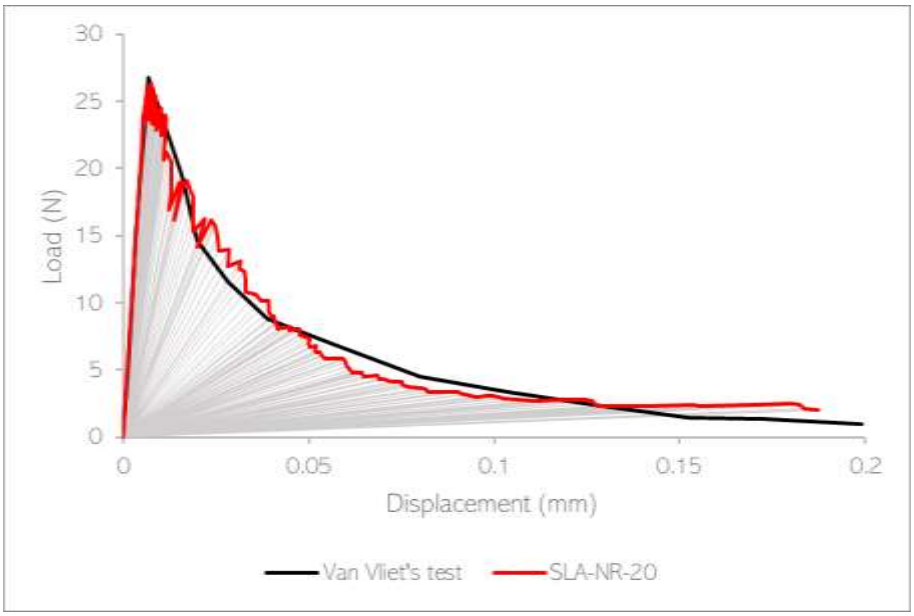

Figure 3.21. Results SLA-NR-20 considering a variable.

III.V Comparison and discussion

The results obtained of the application example demonstrates that the number of teeth used to the saw-tooth diagram are important to have a better approach. To obtain the number of steps that can describe the behaviour of an experiment in the diagram in some points that are difficult to be close. The number of teeth also can be affected in terms of a parameter, as it can be seen in the study with the best results that were obtained in the previous chapter. At first in the method application seems like does not matter the variability of the constant used to divide the Young's Modulus but, as the analysis was becoming more robust, the results were closer to reality.

In terms of having another test with different parameters as the geometry, or the materials that are used to analyze a sequentially linear analysis, the a parameter or the Young's Modulus can be changed to compare if they get a more exact approximation, but speaking of the number of teeth, it can be proved that if the analysis has more teeth, more steps will be iterating between the curve.

Chapter IV
Conclusions

By studying the basis of the Finite Element Method, emphasizing the isoparametric formulation of the 4-node quadrilateral finite element, it was noticed that the discretization of every structure with elastic isotropic characteristics into relatively small elements can approximate the behavior of the entire structure in terms of stress, deformations or displacements.

Consequently, there are several computer programs that can perform a Finite-Element analysis that will make it easier to study the behaviour of certain structure, *e.g.* STKO. However, it cannot be forgotten that these programs will give wrong results if the conditions that are introduced into the software are also wrong. In this regard, it is important to know how the Finite Element Method works.

Moreover, in this thesis was studied that using full and reduced integration for a 4-node quadrilateral element has different effects in the stiffness matrix computation. It was illustrated that the stiffness matrix obtained through reduced numerical integration presents five zero energy deformation modes. Accordingly, a stabilizer stiffness matrix needs to be added to the sub-integrated matrix in order to have a sufficient rank to obtain displacements in different cases of study.

Nevertheless, in terms of nonlinear behaviour structures, SLA was demonstrated to be a method which helps to compute the displacement of different structures by being implemented through FEM. This SLA procedure consists on degrading the material through iterations for approximating the damage on a specific area of the structure. In simple words, Young's Modulus is reduced at each iteration.

To prove that the SLA and the SRI procedures are an adequate analysis strategy if a structure is submitted to proportional load, two different plates were analyzed through this strategy with different properties, as the times that can be reduced each critical element. The results were very closed to the behaviour of the plates previously tested in laboratory.

Moreover, to reduce the Young's Modulus, it was implemented an a parameter that was changing conforming the SLA was moving forward. That means that Young's modulus did not decrease proportionally because the structured demanded a nonlinear approximation.

As a result, for each plate, higher the iterations combined with SLA-SRI, better the results.

For future works using the modified softening law, it can be studied different parameters geometries or even materials to prove that the method works for every nonlinear material implemented in the construction of structures.

This work shows the necessity of bringing attention to the adequacy of certain softening laws for analyzing the global behavior of a structure. This is of particular interest in the SLA procedure, which can be modified relatively easily to follow different softening laws, e.g., bilinear, multilinear, nonlinear, etc. However, the use of certain softening laws must be justified by experimental data.

References

Amezcua, H.R. (2016) Formulation and numerical implementation of an improved finite element model and its application to the study of ancient masonry structures. Master Thesis, UNAM.

Amezcua, H.R. (2022) Numerical approximation of the non-linear behaviour of masonry structures through the finite element method: A computationally efficient strategy. PhD Thesis, UNAM.

ASDEA Software. (2018) STKO | Scientific ToolKit for OpenSees.

Bathe, K. (2006) Finite element procedures (Pearson Education (ed.); 01 ed., Vol. 1). Massachusetts Institute of Technology.

Belytschko, T., Shau, J., Ong, J., Liu, W. K., & Kennedy, J. M. (1984) Hourglass control in linear and nonlinear problems*. 7–38. Computer Methods in Applied Mechanics and Engineering Volume 43, Issue 3.

Gelacio Juárez. (2012) Método de los elementos finitos aplicados a la solución de problemas de la ingeniería estructural. Notas de curso, UAM.

Gupta, K., & Meek, J. L. (1996) A brief history of the beginning of the finite element method. INTERNATIONAL JOURNAL FOR NUMERICAL METHODS IN ENGINEERING, 39, 3761–3774.

Jacquotte, O., Oden, T., & Becker, E. B. (1986) Numerical control of the Hourglass instability. INTERNATIONAL JOURNAL FOR NUMERICAL METHODS IN ENGINEERING, 22, 219–228.

Olivella, X. A. C. (2000) Mecánica de medios continuos para ingenieros: Vol. Second edition.

Orduña, A. R. G. and P. F. (2007) Seismic assessment of historical masonry constructions: comparison of three models of analysis. Revista de Ingeniería Sísmica, SMIS México, 71–88.

Retama, J. (2010). Formulation and approximation to problems in solids by embedded discontinuity models. PhD Thesis, UNAM.

Rots, J. G., Belletti, B., & Invernizzi, S. (2008) Robust modeling of RC structures with an "event-by-event" strategy. Engineering Fracture Mechanics, 75(3–4), 590–614. https://doi.org/10.1016/J.ENGFRACMECH.2007.03.027

Simo, J. C., & F. Armero. (1992) Geometrically Nonlinear Enhanced Strain Mixed Methods and the Method of Incompatible Modes. INTERNATIONAL JOURNAL FOR NUMERICAL METHODS IN ENGINEERING, 33, 1413–1449.

Van Vliet, M. R. A. (2000) Size effect in tensile fracture of concrete and rock. Delft University of Technology.